Ly6c$^+$ "inflammatory monocytes" are microglial precursors recruited in a pathogenic manner in West Nile virus encephalitis

Daniel R. Getts,[1,2] Rachael L. Terry,[1,2] Meghann Teague Getts,[1,2] Marcus Müller,[3] Sabita Rana,[1,2] Bimmi Shrestha,[1] Jane Radford,[1,2] Nico Van Rooijen,[3,4] Iain L. Campbell,[2,3] and Nicholas J.C. King[1,2]

[1]The Discipline of Pathology, School of Medical Sciences, [2]Bosch Institute, Faculty of Medicine, and [3]School of Molecular and Microbial Biosciences, Faculty of Science, The University of Sydney, Sydney NSW 2006, Australia
[4]Department of Molecular Cell Biology, Faculty of Medicine, Vrije Universiteit Medical Center, Vrije Universiteit, 1007 MB Amsterdam, Netherlands

In a lethal West Nile virus (WNV) model, central nervous system infection triggered a threefold increase in CD45^{int}/CD11b$^+$/CD11c$^-$ microglia at days 6–7 postinfection (p.i.). Few microglia were proliferating, suggesting that the increased numbers were derived from a migratory precursor cell. Depletion of "circulating" (Gr1$^-$(Ly6C^{lo})CX3CR1$^+$) and "inflammatory" (Gr1^{hi}/Ly6C^{hi}/CCR2$^+$) classical monocytes during infection abrogated the increase in microglia. C57BL/6 chimeras reconstituted with cFMS–enhanced green fluorescent protein (EGFP) bone marrow (BM) showed large numbers of peripherally derived (GFP$^+$) microglia expressing GR1$^+$(Ly6C$^+$) at day 7 p.i., suggesting that the inflammatory monocyte is a microglial precursor. This was confirmed by adoptive transfer of labeled BM (Ly6C^{hi}/CD115$^+$) or circulating inflammatory monocytes that trafficked to the WNV-infected brain and expressed a microglial phenotype. CCL2 is a chemokine that is highly expressed during WNV infection and important in inflammatory monocyte trafficking. Neutralization of CCL2 not only reduced the number of GFP$^+$ microglia in the brain during WNV infection but prolonged the life of infected animals. Therefore, CCL2-dependent inflammatory monocyte migration is critical for increases in microglia during WNV infection and may also play a pathogenic role during WNV encephalitis.

CORRESPONDENCE
Nicholas J.C. King:
nickk@pathology.usyd.edu.au

Abbreviations used: ANOVA, analysis of variance; BBB, blood-brain barrier; C-L, clodronate-loaded; CNS, central nervous system; D-L, Dil-labeled; H&E, hematoxylin and eosin; IHC, immunohistochemistry; p.i., postinfection; WNV, West Nile virus.

The mechanism resulting in increased numbers of microglia in the central nervous system (CNS) during inflammation has long been debated. Microglia have been shown to proliferate in situ in several synthetic inflammatory models (1–4). In contrast, it is suggested that microglia can differentiate from blood-derived precursors that migrate into the CNS; however, recent reports suggest that this can only occur after radiation-induced "preconditioning" of the brain (5–10). Whether viral infection initiates events resulting in microglial recruitment from the periphery is unknown.

During embryonic development, microglia populate the CNS from myeloid lineage precursors in the BM (11). Much is known about early monocyte lineage precursors, but the differentiation to downstream effector populations in the adult remain poorly defined. Geissman et al. (13) have described two major subsets in the peripheral blood, the "inflammatory" and "circulating" monocyte (12, 14). Inflammatory monocytes express Ly6C^{hi} (Gr1) and the chemokine receptor

D.R. Getts' present address is Department of Microbiology and Immunology, Northwestern University, Chicago, IL.
B. Shrestha's present address is Department of Medicine, Washington University School of Medicine, St. Louis, MO 63110.
M. Müller's present address is Department of Neurology, University of Bonn, 53105 Bonn, Germany.
The online version of this article contains supplemental material.

The Rockefeller University Press $30.00
J. Exp. Med. Vol. 205 No. 10 2319-2337
www.jem.org/cgi/doi/10.1084/jem.20080421

The Journal of Experimental Medicine

CCR2 (12–14). CCR2 and one of its ligands, CCL2, are evidently important in both emigration of these monocytes from the BM and their immigration into inflamed tissues (15, 16). Inflammatory monocytes migrate to the spleen and skin, where they can differentiate into macrophages and Langerhans cells, respectively (6, 13, 17). Circulating monocytes, identified by their low expression of Ly6C in conjunction with CX_3CR_1, are thought to be important in replenishing tissue macrophages during homeostatic conditions (12).

In this study, we have used West Nile virus (WNV) to investigate the in vivo trafficking and differentiation of monocyte/microglia during lethal encephalitis. Although it is clear from previous work that several elements of the systemic immune system work together during WNV infection to control viral growth and dissemination (18–20), it is also apparent that infiltrating $CD11b^+/CD45^+$ myeloid cells contribute to underlying immunopathology observed during WNV encephalitis (21, 22). Although activated microglia have been observed during WNV infection of the brain (19, 23), the contribution of microglia to immunopathology is unknown. Microglia are immune-competent cells of the CNS, comprising up to 20% of the total rodent glial population (24). Resting microglia usually exhibit a ramified dendritic morphology and express low levels of cell surface immune molecules. However, alterations in the microenvironment can result in rapid activation. Activated microglia acquire an amoeboid morphology (25–28), develop an increase in phagocytic ability, exhibit enhanced migratory capacity within the brain, and increase their expression of cell surface glycoproteins including CD45 and MHC-II (26, 29–34).

In this paper, we show for the first time in nonirradiated mice that $Ly6C^{hi}$ inflammatory monocytes migrate in a CCL2-dependent fashion into the WNV-infected CNS, where they develop a microglial phenotype. Inhibition of microglial immigration seen after CCL2 neutralization correlated with enhanced survival of WNV-infected mice. Paradoxically, the titer of WNV in the CCL2-neutralized brains was similar to that observed in nontreated mice, indicating that pathogenesis is not directly related to viral load and implicating CCL2-mediated microglial migration in the pathogenesis of WNV encephalitis.

RESULTS

Microglia become activated and increase in number in response to WNV infection

Sections of brains from C57BL/6 mice infected intranasally with WNV were labeled with GS-lectin and WNV NS-1 antibody to determine the extent of microglial activation and cellular infection. In normal brains, resting microglia exhibit a ramified morphology and express few α-D-galactose residues on their cell surface, making them difficult to detect by immunohistochemistry (IHC) with GS-lectin (35). However, upon activation, expression of α-D-galactose on microglia increases and can be readily detected by IHC. Microglia showed prominent lectin staining in the outer layers of the olfactory bulb on day 3 postinfection (p.i.), corresponding to the appearance of NS-1 staining in this region of the brain (Fig. 1, A and B). Between days 3 and 7 p.i., the morphology of microglia changed. Early activated microglia displayed a dendritic morphology and stained intensely with GS-lectin (Fig. 1 B). However, with progression of infection, as evident by the spread of NS-1 immunoreactivity throughout the brain (Fig. S1, available at http://www.jem.org/cgi/content/full/jem.20080421/DC1), microglia with enlarged cell bodies and retracted processes (stout morphology), as well as those with amoeboid morphology, including rod-shaped and round phagocytic forms, became evident (Fig. 1, C and D; Fig. S1). Rod-shaped microglia were found predominantly in clusters around neurons or near perivascular cuffs and resembled previously described perivascular microglia, also known as Mato cells (Fig. 1, E and F) (36).

Microglia express many markers in common with macrophages. As such, many studies have failed to distinguish correctly between microglia and macrophages. In this study, we used the positive expression of CD11b in conjunction with the differential expression of CD45 antigen on the cell surface using flow cytometry, as originally described by Sedgwick et al. (30). In this way, resting microglia can be differentiated from activated microglia, as well as from macrophages (26). Ramified or resting microglia express a $CD45^{lo}$ phenotype, increasing their cell surface expression to an intermediate (int) level upon activation. Importantly, activated $CD45^{int}$ microglia express a lower level of CD45 than macrophages in the CNS, enabling these two cell types to be differentiated from each other (30).

As expected, the expression of CD45 on leukocytes isolated either from mock-infected mouse brains or at day 0 p.i. was uniformly low (resting microglia [references 26, 30]; Fig. 1 G and not depicted). By day 7 p.i., brains infected with WNV displayed a heterogenous CD45 versus CD11b profile. Relatively few $CD45^{lo}$ microglia were present, whereas a $CD45^{int}$ (activated microglia) population was present and could be distinguished from a significant population of $CD11b^+/CD45^{hi}$ macrophages (Fig. 1 H). The increase in CD45 expression on microglia is indicative of activation of these cells. Analysis of Ly6G and Ly6C expression on these resting and activated microglia (Fig. 1, I and J) showed a significant increase in Ly6C expression on $CD45^{int}$ microglia. The absence of Ly6G expression confirms that these cells are not granulocytes.

Enumeration of microglia by flow cytometry showed that WNV infection resulted in an increase in the absolute number of $CD45^{int}$ microglia (Fig. 1, H and K). Overall microglial cell numbers ($CD45^{lo+int}$) were not statistically different until day 7 p.i. By day 7 p.i., the total numbers of microglia increased by three- to fourfold (Fig. 1 K). The differential contributions of resting and activated microglia are also shown in Fig. 1 K. $CD45^{int}$ cells, virtually absent on day 0 p.i., were found in low numbers on day 3 p.i., correlating with the increase in lectin labeling by IHC. Numbers of $CD45^{int}$ microglia had increased significantly by day 7 p.i. In contrast, numbers of $CD45^{lo}$ microglia had significantly decreased at day 6 compared with day 3 p.i. and were significantly lower than $CD45^{int}$ microglial numbers at day 7 p.i. Because numbers of total microglia at day 6

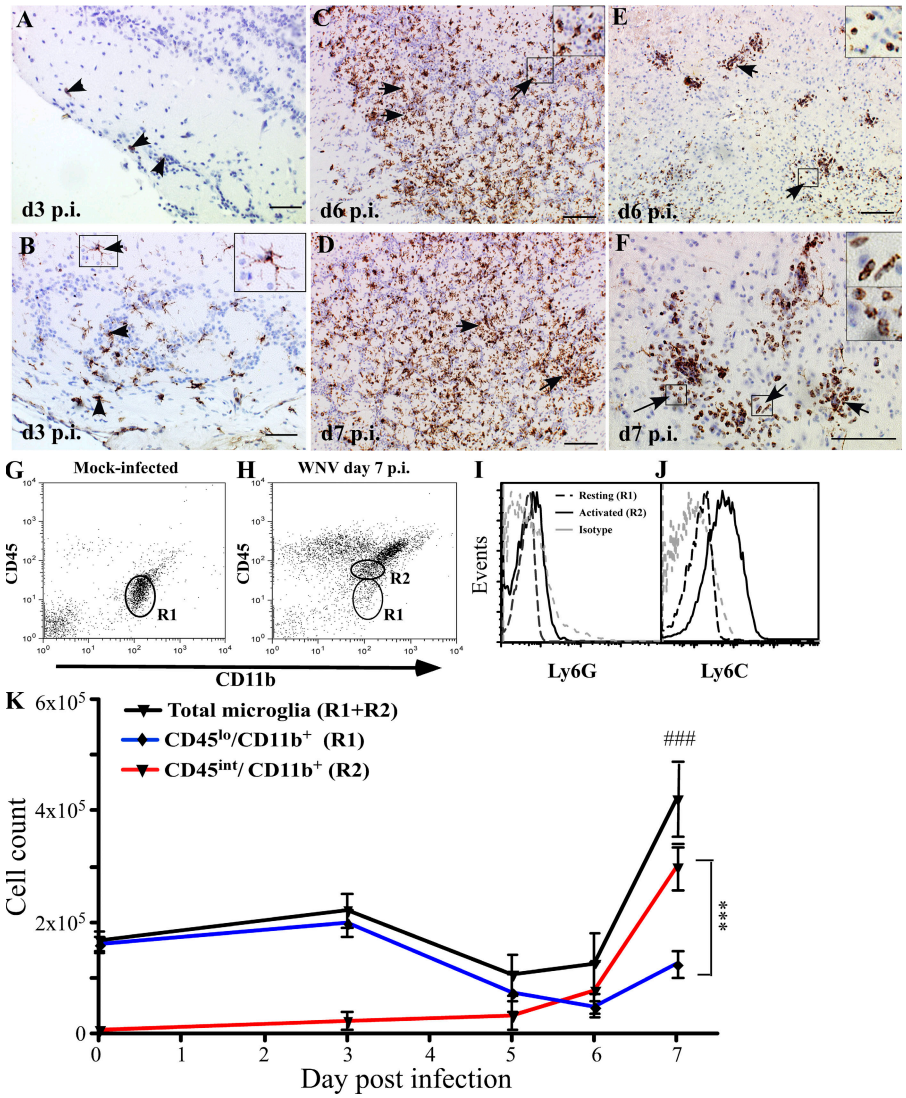

Figure 1. Kinetics of microglial change during WNV infection. WNV NS-1 protein first appeared in the outermost layer of the olfactory bulb on day 3 p.i. (A, arrowheads). Early activated microglia, identified by lectin staining and dendritic morphology, were concurrently detected in the outermost layer on day 3 p.i. (B, arrowheads and enlarged inset of the arrowed box) but nowhere else in the brain. On days 6 and 7 p.i. (C and D), scattered activated microglia (arrows and enlarged inset of the arrowed box) exhibited both amoeboid and intermediate activated morphology in the olfactory bulb. In the brain parenchyma, lectin-positive cells with amoeboid morphology (arrows and enlarged insets of arrowed boxes) were observed surrounding the blood vessels on days 6 (E) and 7 (F) p.i. Bars, 100 µM. Flow cytometry of leukocytes isolated from the whole brain in mock infected (G) showed a predominant population of resting microglia with a classical $CD45^{lo}$ phenotype (R1). By day 7 p.i., significant numbers of activated microglia could be identified by their $CD45^{int}$ expression, as indicated by R2 (H). Analysis of the total microglial population for Ly6G (I) and Ly6C (J) expression showed increased Ly6C expression on activated microglia but no Ly6G expression on resting or activated microglia. Enumeration of total microglia at days 0, 3, 5, 6, and 7 p.i. showed a major increase between days 6 and 7 p.i. (K). Increased numbers of $CD45^{int}$ (activated) microglia could be detected as early as day 3 p.i. (K), with numbers increasing dramatically between days 5 and 7. These changes were temporally independent of decreases in $CD45^{lo}$ (resting) microglial numbers, which declined from day 3 p.i. onwards. Data shown are means ± SD and are representative of three experiments with at least three mice per group. ***, $P < 0.001$, comparing day-7 p.i. $CD45^{lo}$ with day-7 p.i. $CD45^{int}$; ###, $P < 0.001$, comparing day-7 p.i. total microglia with days 0, 5, or 6 p.i. using one-way analysis of variance (ANOVA) with a Tukey-Kramer posttest.

p.i. were not significantly different from those of the earlier time points, this suggests that resting microglia are increasing their CD45 expression (as previously described); however, the significant increase in overall microglial numbers in the brain by day 7 in WNV infection argues that there is either in situ microglial proliferation or external recruitment.

Microglia do not proliferate significantly in situ after WNV infection

As mentioned, several stimuli may induce microglial proliferation, which is measurable by nuclear BrdU incorporation (1–4, 9, 33, 34, 37, 38). However, in some of these studies, mice were exposed to BrdU for several days. This makes it

impossible to exclude the possibility that $BrdU^+$ microglia in these models arose from precursor cells that had proliferated in peripheral sites, such as the BM, and subsequently migrated to the brain. Therefore, groups of WNV-infected mice were pulsed i.v. with BrdU for 3 h on either day 6 or 7 p.i., when maximal increases in microglia were occurring, and killed immediately after the pulse period.

In WNV-infected mice on either day 6 or 7 p.i., the frequency of $BrdU^+$ cells was low. Of the total $BrdU^+$ cells counted in brain sections from infected mice, >70% were localized within perivascular cuffs on both days 6 and 7 p.i., with very few observed in the brain parenchyma (Fig. 2, A, B, and D). Labeling in day-7 p.i. WNV-infected mice not treated with BrdU (Fig. 2 C) or in BrdU-treated mock-infected mice (not depicted) showed virtually no positively labeled cells in any areas of the brain (Fig. 2 D). This was further supported by flow-cytometric analysis, which showed that ~1% of microglia in WNV infection were $BrdU^+$ at day 7 p.i. (Fig. 2, E and F; and Fig. S2, available at http://www.jem.org/cgi/content/full/jem.20080421/DC1). The combination of the very low frequency of $BrdU^+$ microglia in WNV-infected mice, their predominantly perivascular location during the period of greatest increase in activated microglia, and the relatively small reduction in absolute numbers of resting microglia (Fig. 1 K) makes it unlikely that in situ proliferation can account for the large numbers of activated microglia seen at day 7 p.i.

Microglial increases are not caused by breakdown of the blood-brain barrier (BBB)

Breakdown of the BBB may explain the significant burst in numbers of microglia seen in the WNV-infected mouse brain between days 6 and 7 p.i. We investigated the status of the BBB by fibrinogen IHC in the WNV-infected brain at the peak of disease (day 7 p.i.). The presence of fibrinogen has previously been described to detect microvascular leakage in the brain during several distinct neuroinflammatory models and on postmortem brain tissue (39–44). Although all mice infected with WNV had severe leukocyte infiltration and perivascular cuffing, 70% of infected mice (7/10) displayed no detectable fibrinogen immunoreactivity (Fig. 2, J–L), whereas fibrinogen staining in the remaining mice was extremely scant and limited to the luminal side of the endothelium (Fig. 2, M–R). In addition, administration of Evans blue, 1 h before sacrifice on day 7 p.i., showed that BBB breakdown was similarly sporadic, with two out of six mice showing some Evans blue leakage into the brain (Fig. S3, available at http://www.jem.org/cgi/content/full/jem.20080421/DC1). Therefore, similar to other routes of WNV infection (45), the intranasal route of WNV infection causes sporadic BBB breakdown.

Microglial numbers are reduced in monocyte-depleted WNV-infected mice

Microglial infiltration into the brain has been suggested to occur in several models; however, this has not been addressed during viral encephalitis. Recruitment from the peripheral blood to sites of infection in organs other than the brain and their differentiation into effector cells has been shown to involve $Ly6C^+$ or $Gr1^{hi}$ monocytes (13, 14, 46). Interestingly, 31.3 ± 7% of activated microglia expressed Ly6C in WNV-infected mice, compared with 12 ± 0.8% in mock-infected control mice ($P < 0.001$). Furthermore, 7.6 ± 1.5% of resting microglia expressed detectable Ly6C in infected mice, compared with 0.32 ± 0.2% in mock-infected control mice ($P < 0.001$). To determine whether blood-derived monocytes are microglial precursors during WNV infection, we depleted blood monocytes with clodronate-loaded (C-L) liposomes. It has previously been shown that liposomes do not deplete macrophages in the brain parenchyma (47, 48). Although perivascular cuffs were evidently resistant to C-L liposome depletion in WNV-infected mice (Fig. 3, A–L), we additionally used DiI-labeled (D-L) liposomes to further confirm visually that liposomes do not have access to the CNS during WNV infection (Fig. 3, M–X and top right insets). After injection, D-L liposomes were abundantly localized to the splenic marginal zones in both infected and mock-infected mice (Fig. 3, M–T). In contrast, no D-L liposomes were found in the brains of either day-7 WNV-infected mice (Fig. 3, U–X) or mock-infected mice (Fig. 3 X, bottom left inset), confirming that liposomes do not cross the BBB. This further supports the data in the previous section, indicating that little or no BBB breakdown occurs in this model. Overall, these data support previously published reports and indicate that this method of depletion primarily affects peripheral monocyte populations, especially the inflammatory monocyte compartment (Fig. S4, available at http://www.jem.org/cgi/content/full/jem.20080421/DC1) (49).

Clodronate liposome treatment of WNV-infected mice 1 d before infection and then every other day onwards resulted in significantly reduced numbers of microglia in the brain, as detected using flow cytometry, on day 7 p.i., compared with WNV-infected mice without treatment or treated with nondepleting null liposomes (Fig. 3 Y). As C-L liposomes do not delete any myeloid cells behind the BBB but cause a significant reduction in the number of microglia in the brain, this strongly suggests that the increased numbers of microglia in the brain in WNV encephalitis are derived from blood monocytes.

Increased microglial numbers in WNV infection are derived from the blood

To further investigate possible microglial precursors during WNV infection, we used the cFMS-EGFP mouse. cFMS is the colony stimulating factor receptor 1, CD115, and is largely restricted to cells of the macrophage lineage (50). Microglia in the normal brain are mostly quiescent and thus radio resistant. Therefore, chimeric mice were made, in which BM from C57BL/6-7.2fms-EGFP transgenic (CD45.2) mice was used to reconstitute γ-irradiated C57BL/6 congenic B6.SJL-$Ptprc^aPep3^b$/BoyJ (CD45.1) mice (Fig. S5, A–C, available at http://www.jem.org/cgi/content/full/jem.20080421/DC1). This chimera allowed us to differentiate between resident (GFP^-) and infiltrating (GFP^+) microglia (50).

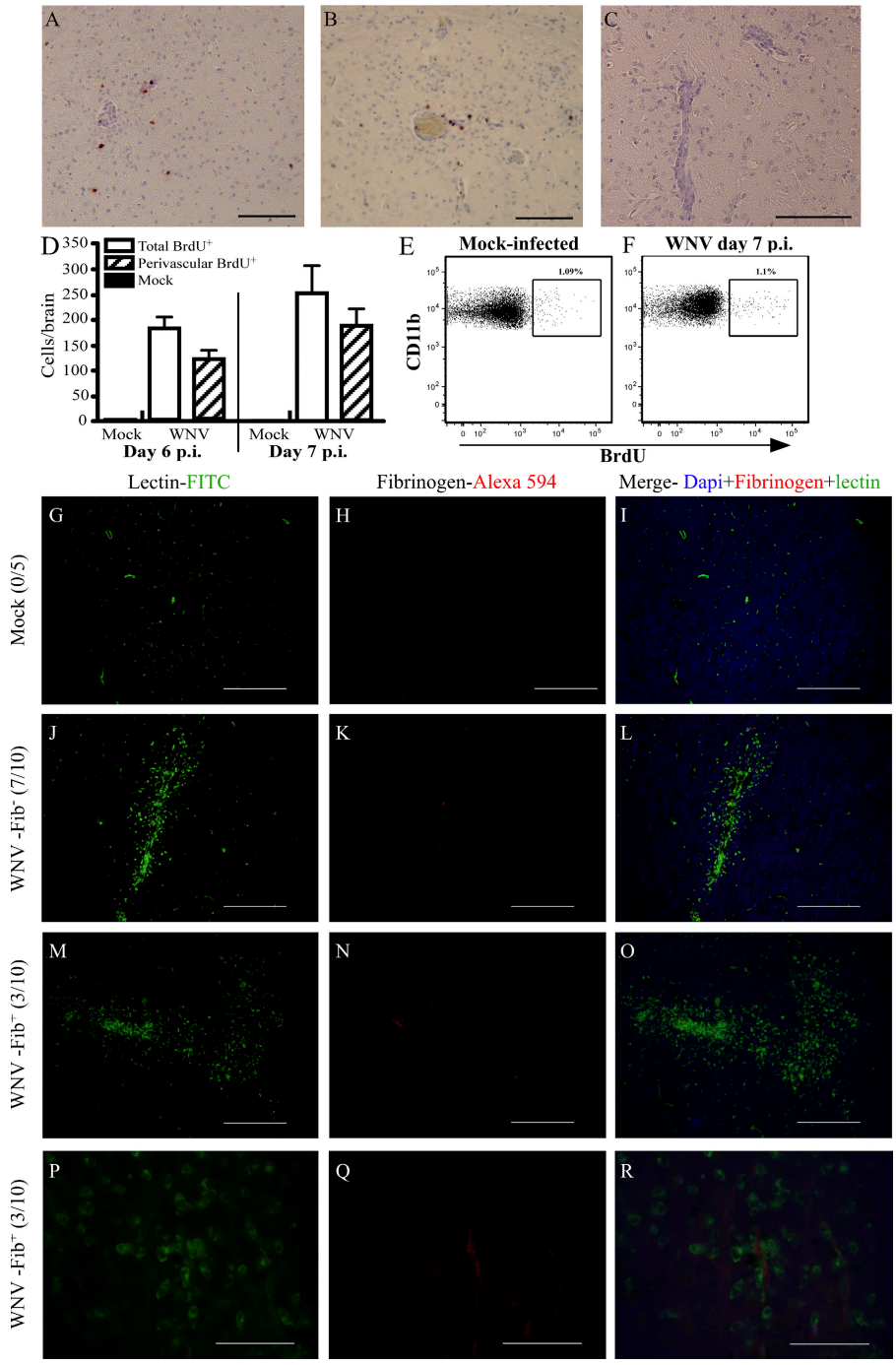

Figure 2. There is little cellular proliferation and negligible BBB disruption during WNV encephalitis. Mice were treated with BrdU for 3 h before sacrifice. Routine IHC for BrdU showed that BrdU+ cells localized predominantly to the perivascular cuff on days 6 (A) and 7 (B) p.i. This was not seen in mock-infected mice or mock BrdU-treated WNV-infected mice (C). Enumeration of BrdU+ cells on histological sections showed that >70% of all BrdU+ cells were perivascularly localized (D). The percentage of proliferating microglia was also determined by flow cytometry (E and F). Approximately 1% of microglia in WNV-infected and mock-infected mice were seen to be BrdU+ (E and F). To test the status of the BBB, fibrinogen IHC was performed on 10 WNV-infected mice and 5 mock-infected mice. Fibrinogen was not detected in any mock-infected mice at day 7 p.i. (0/5; G–I). Furthermore, 7/10 WNV-infected mice also failed to exhibit any evidence of fibrinogen leakage (J–L). In the three mice where fibrinogen labeling was detected, staining was scant and limited to the luminal surface of vessels (M–O, 20×; P–R, 100× images of M–O). Data shown are means ± SD. Data from BrdU experiments are representative of two experiments with at least five mice per group. Bars: (A–C) 100 µM; (G–O) 200 µM; (P–R) 50 µM.

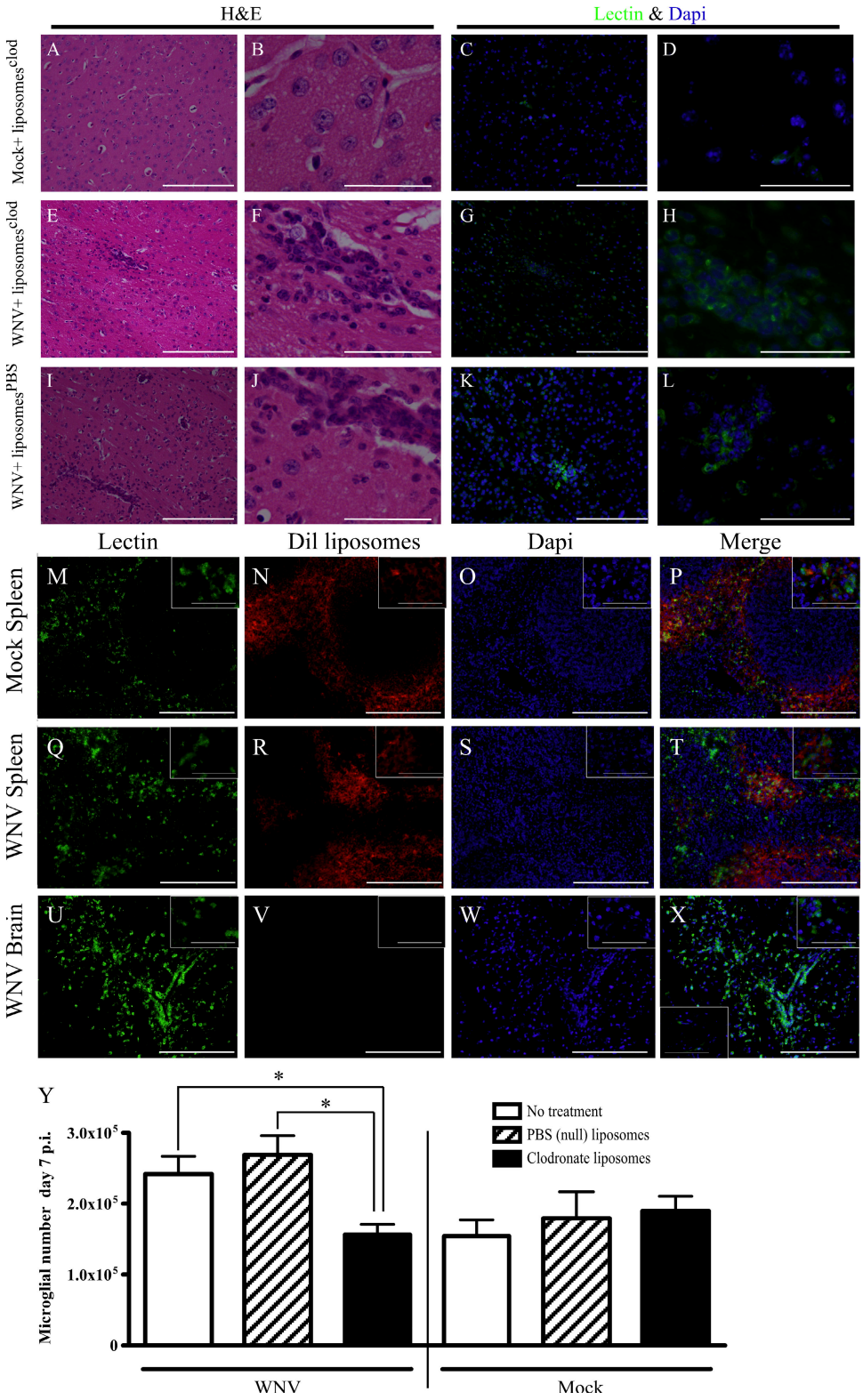

Figure 3. C–L liposomes do not enter the WNV-infected CNS. Liposomes loaded with clodronate were injected i.v. at day 7 p.i. and, 6 h later, mice were killed. Hematoxylin and eosin (H&E) staining of brain sections showed no perivascular cuffing in mock-infected animals (A and B). In contrast, distinct perivascular cuffs were observed in the WNV-infected C-L liposome–treated group (E and F) and the WNV-infected PBS liposome-treated group (I and J). To confirm that the cells within these cuffs were of myeloid lineage, we stained sections, consecutive to those stained with H&E, with lectin. Lectin staining in brain sections from mock-infected mice confirmed the absence of perivascular cuffing (C and D). In contrast, most of the cells within

Histological examination revealed that both GFP$^+$ perivascular macrophages (Fig. 4 A, white arrow) and GFP$^+$ parenchymal ramified microglia (Fig. 4 B) accounted for a small percentage of cells in the mock-infected brain, which is consistent with previous work (Fig. 4, G and H) (7). Similar to C57BL/6 mice, WNV-infected chimeric mice developed encephalitis and were moribund by day 7 p.i. (unpublished data). WNV-infected cFMS-EGFP chimeras displayed numerous GFP$^+$ cells in all regions of the brain by day 7 p.i. (Fig. 4, C and D). Of particular note, the distribution of these GFP$^+$ cells was mostly within perivascular cuffs (Fig. 4 C and inset). In addition, cells nearest the center of the perivascular cuff appeared to have a round monocytic morphology (Fig. 4 C, inset, white arrow), whereas those nearer to the brain parenchyma on the periphery of the perivascular cuffs were more rod shaped (inset, red arrow), suggesting monocyte differentiation as cells enter the parenchyma.

Flow cytometric analysis at day 7 p.i. confirmed that at least 50–75% of activated microglia (CD45^{int}/CD11b$^+$/CD11c$^-$) expressed GFP, indicating that they were peripherally derived (Fig. 4, E and G). Furthermore, at this time point, 75% of these activated GFP$^+$ microglia also expressed the inflammatory monocyte-associated Gr1 (Ly6C; Fig. 4, F and I). In contrast, most resting microglia (CD45^{lo}/CD11b$^+$/CD11c$^-$) from both mock-infected and WNV-infected chimeras were GFP$^-$, indicating that they were of resident origin (mock infected, 93 ± 3.0%; WNV-infected, 88 ± 3.9%; Fig. 4 H). Adding together the data in Fig. 4 (G and H, right), it can be seen that the total number of GFP$^-$ microglia (i.e., activated and resting) in WNV-infected mice was not significantly different from the total number of GFP$^-$ microglia in mock-infected mice. This suggests that proliferation of microglia in situ in the brain is unlikely to be the major mechanism for increased microglial numbers during WNV encephalitis. Furthermore, the proportion of GFP$^+$ CD45^{int} microglia expressing GR1 in the WNV-infected mouse supports the differentiation of these microglia from a blood-derived precursor, specifically the GR1-expressing inflammatory monocyte.

Adoptively transferred Ly6c^{hi}, not Ly6C^{lo}, cells traffic to the CNS within 12 h of transfer

It has previously been reported that the ability of inflammatory monocytes to penetrate the CNS in chimeric mice is caused by irradiation preconditioning of the CNS. Therefore, because there was negligible breakdown of the BBB in this viral model, we further investigated the ability of inflammatory monocytes to penetrate the CNS using tracking techniques in nonirradiated mice.

First, we tested the ability of inflammatory monocytes (Ly6C^{hi}/CD11b$^+$/cFMS-EGFP$^+${CD115$^+$}) and circulating monocytes (Ly6C^{lo}/CD11b$^+$/cFMS-EGFP$^+${CD115$^+$}) to traffic to the CNS. To do this, we adoptively transferred 10^6 EGFP$^+$/CMTMR–cell tracker orange$^+$ BM-derived inflammatory monocytes (Ly6C^{hi}) together with 10^6 EGFP$^+$/CMTMR–cell tracker orange$^-$ BM-derived circulating monocytes (Ly6C^{lo}) at day 6.5 p.i. (Fig. 5, A–D). 12 h later, the presence of these cells in the brain was investigated using flow cytometry (Fig. 5, E–I). Although recovery of adoptively transferred cells was low, the number of EGFP$^+$ cells in the brain was significantly greater in the WNV-infected animal (Fig. 5 F, 0.03%) than in the mock-infected mouse (Fig. 5 G, 0.005%). Cell tracker orange$^+$ GFP$^+$ Ly6C^{hi} cells comprised >90% of adoptively transferred cells isolated from the brain (Fig. 5 I). Interestingly, both CD45^{int}- and CD45^{hi}–expressing GFP$^+$ cells were isolated from the WNV-infected brain (Fig. 5 H), suggesting that Ly6C^{hi} precursors may differentiate into either microglia or macrophages. This was also seen when we transferred GFP$^+$ Ly6C^{hi} and GFP$^+$ Ly6C^{lo} monocytes separately into mock-infected mice (Fig. 5, J and L–N) or WNV-infected mice at day 6 p.i. (Fig. 5, K and O–Q).

As a second test to confirm the role of inflammatory monocytes as microglial precursors during WNV encephalitis, we used an in vivo bead labeling system that was previously described (51, 52). Using clodronate liposome depletion at day 5.5 p.i. with FITC polystyrene bead injection 12 h later, we were able to recapitulate the stable labeling of circulating Ly6C^{hi} inflammatory monocytes in WNV-infected mice (Fig. 6, A–F), as was previously described in uninfected mice (14, 51). In brief, injection of FITC beads alone into WNV-infected mice at day 6 p.i. resulted in the stable labeling of GR1^{lo} monocytes in the circulation (Fig. 6, B and D). In contrast, prior C-L liposome–mediated depletion before bead infusion resulted in stable labeling of GR1^{hi} or inflammatory monocytes (Fig. 6, C and E).

Flow cytometric examination of the WNV-infected brain at day 7 p.i. in mice where inflammatory monocytes were labeled with beads after C-L liposome treatment revealed a strong bead$^+$/CD45^{int}/CD11b$^+$/CD11c$^-$ population of microglia (Fig. 6 J), which was absent in non–bead-treated (Fig. 6 H)

the perivascular cuff were lectin$^+$ in both the WNV-infected C-L liposome–treated (G and H) and the PBS liposome-treated (K and L) groups. To further ensure that C-L liposomes used to deplete circulating monocytes did not enter the brain, we injected D-L liposomes at day 7 p.i. DiI was found in the marginal zones of mock- (M–P) and WNV (Q–T) -infected mouse spleens. However, no D-L liposomes were found in the WNV-infected brain (U–X) or the mock-infected brain (X, bottom left inset). Top right insets are higher power views of cells in representative fields. Depletion of monocytes from the blood compartment with C-L liposomes from 1 d before infection and then every other day onwards resulted in a significant reduction in the numbers of microglia in WNV-infected mice compared with WNV-infected mice treated with null liposomes or mock-treated, as detected by flow cytometry (Y). Data shown are from at least three mice per group and are representative. C-L liposome depletion data are means ± SD and are representative of three experiments with at least three mice per group. *, $P < 0.05$ using a two-tailed T test. Bars: (A, C, E, G, I, K, and M–X) 200 μM; (B, D, F, H, J, L, and insets) 50 μM.

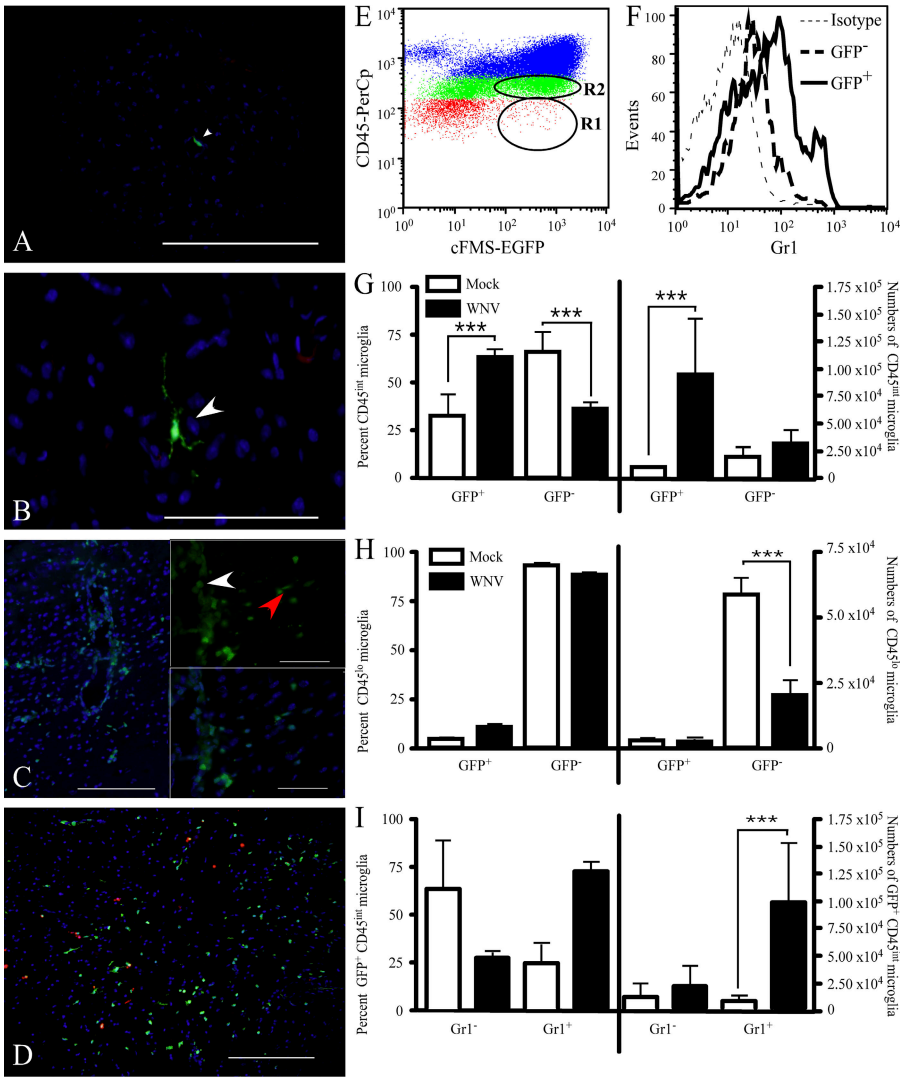

Figure 4. Histology and flow cytometry of WNV-infected cFMS-EGFP chimeras. Reconstitution of γ-irradiated C57BL/6 congenic B6.SJL-Ptprc^{a}Pep3^{b}/BoyJ (CD45.1) mice with cFMS-EGFP BM resulted in chimeras in which a small number of GFP^{+} cells were present in the CNS of mock-infected mice. Histologically, GFP^{+} cells (white arrowheads) were usually seen around the perivascular space (A); however, a small number of ramified microglia expressing GFP were seen in the parenchyma (B). During WNV infection, a large influx of GFP^{+} cells was seen, in most cases located to the perivascular cuff (C, 20× magnification). Insets (100× magnification of the same field) show recruited round GFP^{+} cells near the vessel lumen (white arrowhead) and rod-shaped GFP^{+} cells closer to the parenchyma (red arrowhead). Gr1 (D, red) staining of chimeras clearly showed several Gr1^{+}/cFMS^{+} cells in the brain (D, yellow). Using flow cytometry (E), it was clear that a large proportion of GFP^{+} cells were CD45^{int} microglia (R2) and CD45^{hi} macrophages (blue dots), as well as Gr1^{+} (F). Significantly more (approximately fourfold) CD45^{int} microglia were GFP^{+} at day 7 p.i., compared with mock-infected mice (G), whereas there were significantly fewer GFP^{-} CD45^{lo} resting microglia at day 7 p.i., compared with mock-infected mice (H). Significantly more (at least fourfold) GFP^{+} CD45^{int} microglia were Gr1^{+} at day 7 p.i., compared with mock-infected mice (I). Gr1 data shown are means ± SD and are representative of four experiments with at least three mice per group (***, $P < 0.001$, two-tailed unpaired *t* test). Bars: (A and D) 200 µM; (B and C) 100 µM; (insets) 50 µM.

and bead-only–treated WNV-infected controls (Fig. 6 I). This data clearly suggests that the migration of bead^{+} blood monocytes into the brain and subsequent differentiation into microglia is a very rapid event. As this has not been described, and to ensure that these CD45^{int}/CD11b^{+} bead^{+} cells isolated from the brain were not just recently migrated nondifferentiated blood monocytes, we compared the expression of GR1, MHC-II, and the costimulation molecule CD86 on bead^{+} CD45^{int}CD11b^{+} brain microglia and bead^{+} inflammatory monocytes in the circulation (Fig. 6, I–K). The pattern of GR1 expression on bead^{+} microglia was decreased, compared with circulating bead^{+} inflammatory monocytes, suggesting that Ly6C is down-regulated when monocytes enter the inflamed CNS (Fig. 6 K). Levels of both MHC-II and CD86, in contrast, were higher on bead^{+} microglia compared with bead^{-} or bead^{+} circulating inflammatory monocytes (Fig. 6, L and M).

These adoptive transfer and bead-tracking experiments demonstrate the traffic of inflammatory monocytes in nonirradiated

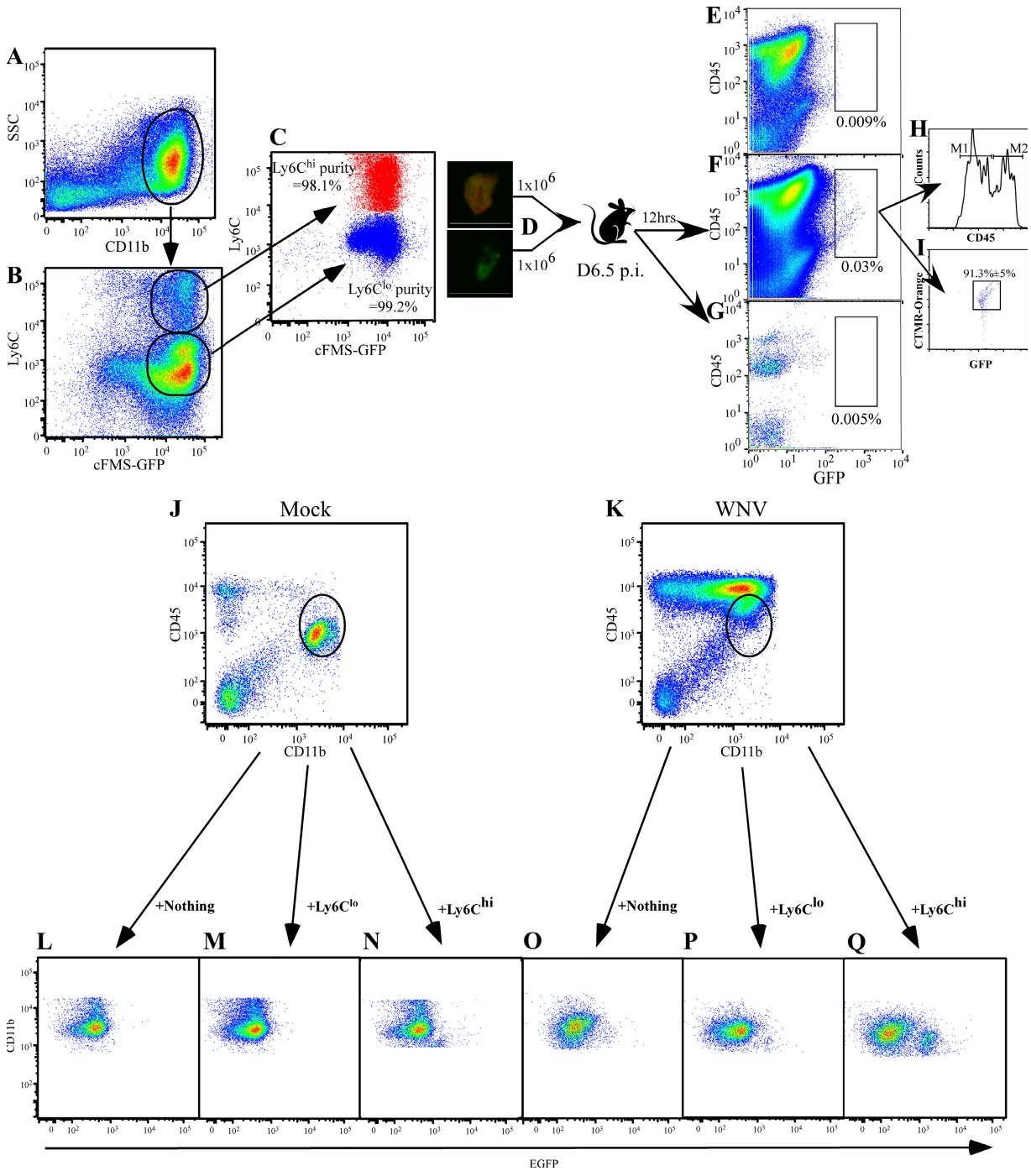

Figure 5. Adoptively transferred Ly6C^{hi} monocytes traffic into the WNV-infected CNS. Ly6C^{hi}/CD11b^{+}/GFP^{+} and Ly6C^{lo}/CD11b^{+}/GFP^{+} BM cells were sorted as shown (A–C) from day 6 WNV-infected cFMS-EGFP transgenic mice. Ly6C^{hi} monocytes were labeled as described in Materials and methods with CTMR–cell tracker orange (D). A 1:1 ratio of Ly6C^{hi}/Ly6C^{lo} cells was intravenously injected into WNV-infected mice on day 6.5 p.i. or into mock-infected mice, whereas some mice received no cells. Leukocytes were isolated from the brains of these WNV-infected mice receiving no cells (E) and from WNV-infected (F) and mock-infected (G) brains 12 h after transfer. GFP^{+} cells were only found in the CNS of WNV-infected mice (F), with the adoptively transferred cells expressing differential levels of CD45 (H) as indicated by markers M1 (CD45^{int}) and M2 (CD45^{hi}). More Ly6C^{hi} (GFP^{+}/CTMR cell tracker orange^{+}) BM cells were found to track to the WNV-infected brain than Ly6C^{lo} (GFP^{+}/CTMR–cell tracker orange^{-}) BM cells (I). This was also observed when we injected these populations of cells separately into mock-infected (J and L–N) or WNV-infected mice (K and O–Q). Data are representative of two experiments with at least four mice per group. Bars, 50 µM.

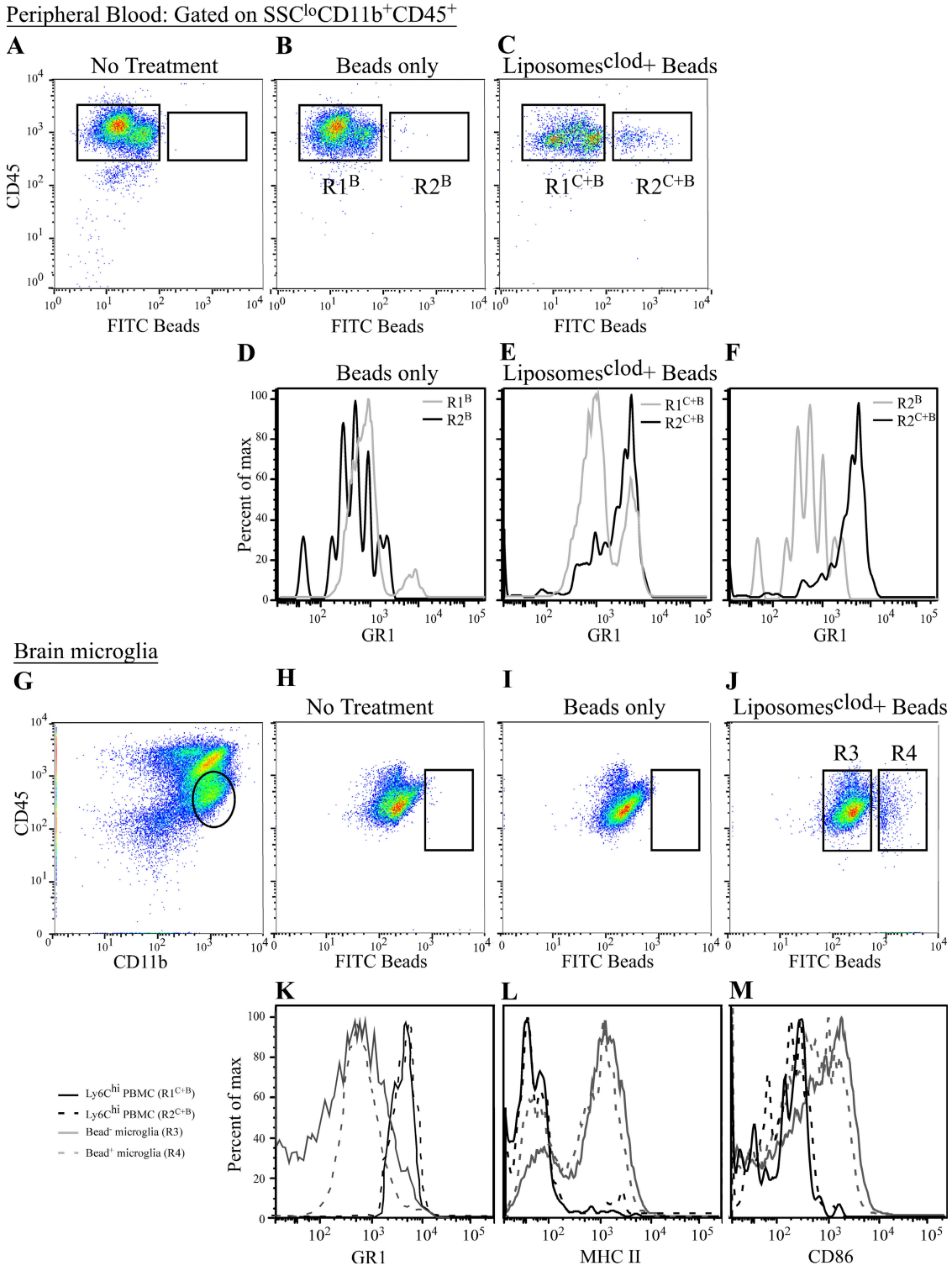

Figure 6. Bead-labeled inflammatory monocytes, not GR1^{lo} monocytes, traffic into the WNV-infected brain. As a second method for trafficking monocytes, we stably labeled peripheral Ly6C^{hi} monocytes, as previously described (14, 51) (A–F). WNV-infected mice receiving no FITC beads had no circulating bead$^+$ cells (A). WNV-infected mice that received only beads with no prior macrophage depletion with C-L liposomes only had beads inside Ly6C^{lo} monocytes (R2^B; B and D). In contrast, C-L liposome depletion in WNV-infected mice before bead injection resulted in the labeling of Ly6C^{hi} inflammatory monocytes (R2^{C+B}; C, E). The successful labeling of Ly6C^{hi} versus Ly6C^{lo} is confirmed by overlaying R2^B and R2^{C+B} (F). Finally, when we looked for the presence of beads in microglia (gated as shown in G) in WNV-infected mice, we found none in the non–bead-treated group (H) or the group in which Ly6C^{lo} peripheral monocytes were labeled with beads (I). However, in WNV-infected mice where we labeled the Ly6C^{hi} monocyte population with beads

mice and show clearly that the large burst of microglial numbers seen in the WNV-infected brain is caused by the recruitment of inflammatory monocytes and is not the result of radiation-induced changes in the CNS. Furthermore, these data show that inflammatory monocyte differentiation into microglia may occur in a shorter time frame than originally considered (12, 34).

WNV infection triggers CCL2 production, which attracts inflammatory monocyte, microglial precursors

CCL2 has been implicated in the egress of monocytes from BM (15, 16). We hypothesized that CCL2 may be involved in this process during WNV infection. Intranasal WNV infection of the CNS triggered the secretion of substantial amounts of CCL2 protein in the brain, beginning on day 5 and increasing until the time of death (Fig. 7 A). The kinetics of these high brain levels were mirrored by much lower levels in the serum (Fig. 7 A). Message for this chemokine is shown in Fig. 7 B (i) near perivascular cuffs by CCL2 mRNA in situ hybridization in the brain. Labeling for CCL2 protein in WNV-infected brains confirmed the presence of CCL2 protein at the perivascular cuff. However, costaining for viral antigen (NS-1), lectin, and CCL2 protein showed that many, though not all, virus-infected neurons and some uninfected neurons were $CCL2^+$, whereas only occasional microglia were $CCL2^+$, suggesting that viral-infected neurons are a major source of CCL2 during WNV infection (Fig. 7 B, ii–v).

The data in the previous paragraph suggest that the CNS was the source of the serum CCL2 and that this induced the egress and observed migration of BM monocytes to the CNS. To test this, we injected CCL2-neutralizing antibody to inhibit both BM egress and CNS trafficking in cFMS-EGFP chimeras. Fig. 7 C shows a statistically significant reduction in the number of $GFP^+/CD11b^+/CD45^{int}$ (reduced to 31%) and $CD45^{lo}$ (reduced to 29%) immigrating microglia isolated from the CNS on day 7 p.i. after CCL2 neutralization, compared with isotype antibody-treated WNV-infected mice. This indicates that a major factor in the immigration of microglia is CCL2. This was not attributable to irradiation because nonirradiated WNV-infected mice (Fig. 7, D–G) also showed a reduction of up to 50% of total microglial numbers (Fig. 7 G). This reduction was mostly accounted for by the reduction of $Ly6C^{hi}$ microglia to ~20% of the levels seen in control isotype antibody-treated mice (Fig. 7 G).

This was further reflected in chimeric mice by the analysis of $GFP^+/CD11b^+$ monocytes in the blood and BM, using the gating strategy illustrated (Fig. 8, A–C). As expected, in the BM, significantly more $Gr1^{hi}$ cells were retained in the CCL2-neutralized compared with the isotype antibody–treated mice, whereas $Gr1^{lo}$ cells were not statistically different between these groups (Fig. 8 D, right), confirming previous studies (15). However, CCL2 neutralization significantly increased the $GR1^{hi}$ cell numbers in the blood but had little effect on the $GR1^{lo}$ monocyte numbers (Fig. 8 D, left). Thus, $Gr1^{hi}$ cells are evidently inhibited from immigrating into the brain in CCL2-neutralized WNV-infected mice, both at the level of the BBB and during egress from the BM. In contrast, over this short period of time (12 h), no changes were observed in blood and BM monocyte compartments after CCL2 neutralization of mock-infected mice (Fig. S6, available at http://www.jem.org/cgi/content/full/jem.20080421/DC1). This data indicates the importance of CCL2 in the trafficking of microglia from the BM to the brain during WNV encephalitis.

CCL2 neutralization prolongs survival

In initial CCL2 neutralization experiments, neutralized mice displayed reduced disease-induced behaviors, including seizures, piloerection, and hunching (unpublished data). Treatment of infected mice with neutralizing antibody over several days resulted in significantly prolonged survival time, compared with infected mice receiving either isotype antibody or PBS alone (Fig. 8 E). Importantly, CCL2 neutralization had no effect on the titer of WNV in these mice, despite their increased survival (Fig. 8 F). This indicates that the immigrating $Ly6C^{hi}$ microglia arising from the BM are pathogenic in WNV encephalitis. Importantly, these data also discount a role for these cells in dissemination of WNV to the brain in this model.

DISCUSSION

The role of monocyte trafficking as a mechanism for microglial cell replenishment has been debated for some time. This has been fueled by the inability to identify microglia from other macrophage populations found in diseased brains. Using several methods, we have highlighted a critical role for peripheral $Ly6C^{hi}$ inflammatory monocytes and the chemokine receptor ligand CCL2 in the ontogeny of microglia during fatal WNV infection of the brain.

Although it is often argued that microglial proliferation is the mechanism behind increased microglial cell numbers seen during CNS inflammation, the low level of proliferation observed during WNV infection in conjunction with the ability of peripheral depletion of both classical and circulating monocytes to significantly reduce the numbers of microglial cells in WNV-infected brains at day 7 p.i. suggest that the recruitment of a peripheral microglial precursor plays an important role in WNV encephalitis.

The peripheral blood contains two monocyte subsets, the inflammatory and circulating monocytes (6, 13, 14, 17, 46, 49, 51). Inflammatory monocytes are distinguished from circulating monocytes by their differential expression of the Ly6C portion of the Gr1 complex (6, 13, 17, 49). The similar expression of Ly6C on several $CD45^{int}$ microglia isolated from the WNV-infected brain implicates inflammatory monocytes as a microglial precursor pool (13, 14, 49).

after C-L depletion, we found microglia-containing FITC beads (J). Furthermore, bead$^+$ microglia showed down-regulated GR1, compared with bead$^+$ inflammatory monocytes (K), suggesting down-regulation upon entry in to the CNS. Finally, these bead-labeled monocyte-derived microglia had also up-regulated their expression of MHC-II (L) and CD86 (M) upon entry into the brain.

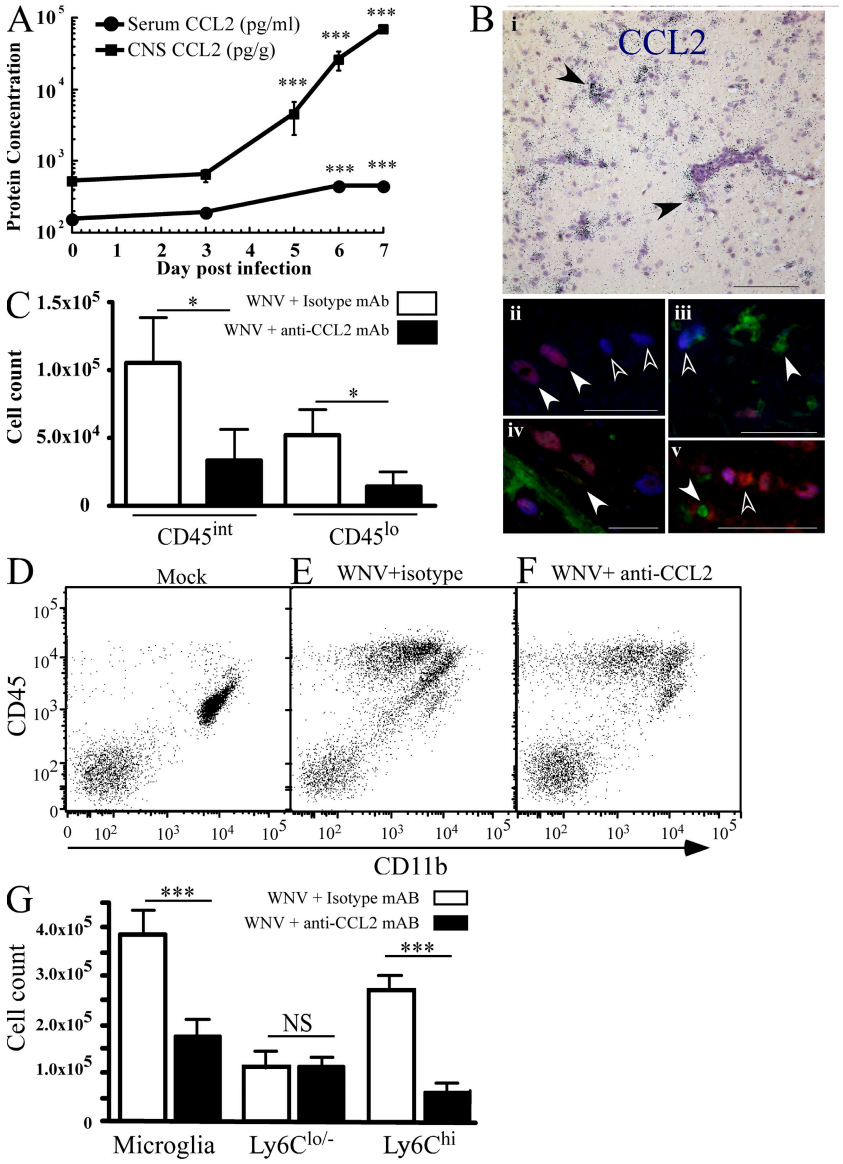

Figure 7. CCL2 protein kinetics and neutralization during WNV infection. Using a multiplexed cytokine bead array, we measured both the serum and brain levels of CCL2. The level of CCL2 protein increased throughout infection in both brain and serum (A). CCL2 mRNA in the brain of five WNV-infected mice on day 7 p.i. was often localized to perivascular cuffs (B, i, black arrowheads). Fluorescent antibody labeling for CCL2 protein (red) and NS-1 (blue) showed that most cells expressing CCL2 were infected neurons (B, ii–iv; ii, white arrowheads). Not all infected neurons expressed CCL2 (B, ii and iii, white outlined arrowheads) and some uninfected neurons expressed CCL2. (B, v, white outlined arrowheads). The addition of lectin staining (green; B, iii–iv) showed that occasional perivascular microglia also expressed CCL2 faintly (B, iv, white arrowhead), whereas most microglia evidently did not (B, iii and v, white arrowheads). CCL2 in WNV-infected EGFP-cFMS chimeras was neutralized with intraperitoneal CCL2-neutralizing monoclonal antibody, resulting in a significant reduction in immigrant (GFP^+) microglia at day 7 p.i. (C). We also determined whether this was also observed in nonirradiated mice (D–G). In nonirradiated WNV-infected mice, CCL2 neutralization (F) resulted in significantly reduced numbers of microglia, accounted for by drastic reduction in $Ly6C^{hi}$-expressing cells (G), which was not observed in mock- (D) and WNV (E) -infected mice. Data shown are means ± SD and are representative of at least two experiments with at least three mice per group. CCL2 broad array data are representative of three different experiments with at least three mice per group. Statistical analysis of CCL2 protein data was conducted using one-way ANOVA with a Tukey-Kramer post test. Neutralization experiments were analyzed using a two-tailed unpaired *t* test comparing neutralized to nonneutralized WNV infected mice. *, $P < 0.05$; ***, $P < 0.001$. Bars: (B, i) 200 µM; (B, ii–iv) 50 µM.

BM chimeras have been successfully used to monitor microglial behavior in several disease models and allow for the differentiation of resident and immigrant microglia (5, 7, 8). However, these studies relied on the expression of β-actin in donor BM in conjunction with IHC directed against antigens such as CD11b and IBA-1 (5, 8). As these antigens are expressed equally in macrophages and microglia, definitive identification of microglia and distinction from macrophages

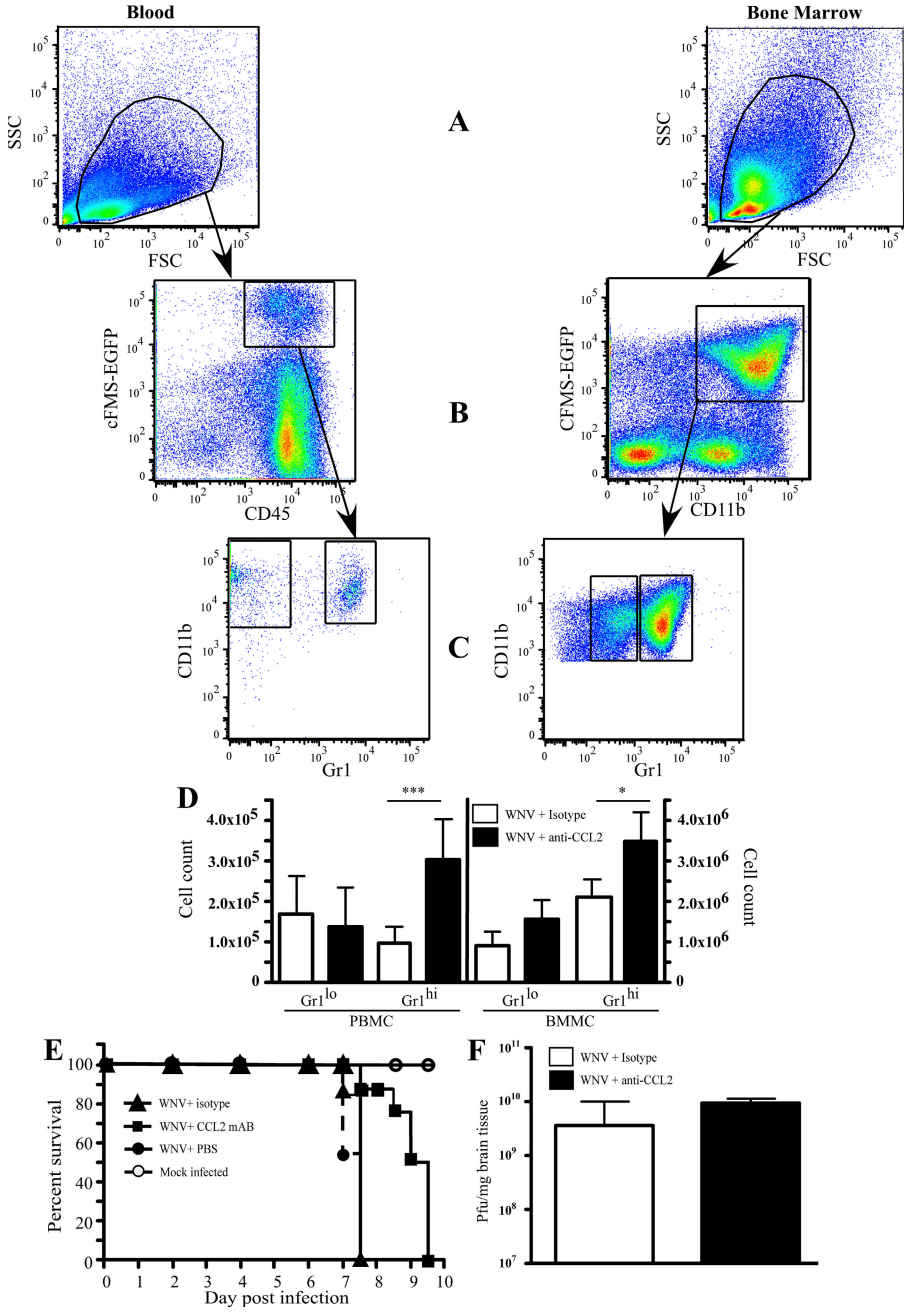

Figure 8. CCL2 neutralization sequesters Gr1^{hi} monocytes in the BM and blood of WNV-infected mice and prolongs the life of WNV-infected animals. Monocyte populations in the BM (BM-derived monocyte) and peripheral blood (peripheral blood monocyte) were investigated by flow cytometry, based on the expression of EGFP-cFMS in conjunction with a cocktail of antibodies, including CD11b and CD45, using gating strategies indicated in A, B, and C. CCL2 neutralization in WNV-infected EGFP-cFMS chimeras resulted in significant increases in Gr1^{hi} (inflammatory monocytes) in both the BM and peripheral blood (D), as well as significantly prolonging the life of WNV-infected mice (E), compared with WNV-infected mice either treated with isotype control mAb or PBS during infection. Plaque assays (F) showed that CCL2 neutralization had no significant impact on the viral titer on day 7 p.i. Data shown are means ± SD and are representative of two different experiments with four mice per group. Neutralization experiments were analyzed using a two-tailed unpaired *t* test comparing neutralized to nonneutralized WNV-infected mice. *, $P < 0.05$; ***, $P < 0.001$. Kaplan-Meyer survival curves are representative of the results of two separate experiments with 10 mice per group in each. Data were analyzed using Prism Chi test ($P < 0.001$).

during inflammation is impossible. In the present study, BM from mice expressing EGFP on the cFMS promoter (CD115) were used as donors for chimeras. In conjunction with flow cytometry staining for CD45 antigen, this allowed us not only to delineate between resident (GFP$^-$) and immigrating (GFP$^+$) myeloid cells but also definitively to distinguish between CD45^{hi} macrophages and CD45$^{lo/int}$ microglia (29, 50, 53). Infected cFMS-EGFP chimeras displayed widespread leukocyte

Table I. Antibodies used in this study

Antibody	Method	Concentration	Source	Isotype	Source
WNV-NS-1-biotin+	IHC	1:100	R. Hall (University of Queensland, Brisbane, Australia)	Mouse IgG1	BioLegend
GS-lectin-biotin+/FITC	IHC	1:50	Sigma-Aldrich	N/A	N/A
CD11b-APC/PE/APC-CY7/Alexa-700	FC	1:100	BD Biosciences/ BioLegend	Rat IgG_{2b}	BD Biosciences/ BioLegend
CD45-PerCP	FC	1:100	BD Biosciences	Rat IgG_{2b}	BD Biosciences
Ly6C-FITC/ Biotin	FC	1:100	BD Biosciences	Rat IgM	BD Biosciences
Ly6G-PE	FC	1:100	BD Biosciences		BD Biosciences
GR1-biotin/APC-Cy7/ Pacific blue	FC/IHC	1:100	BD Biosciences/ BioLegend	Rat IgG_{2b}	BD Biosciences/ BioLegend
CD11c-biotin+/PE-Cy7	FC	1:150	BD Biosciences/ Biolegend	Hamster IgG	BD Biosciences/ BioLegend
CCL2-LEAF	Neut	100 µg per mouse	BioLegend	Hamster IgG-LEAF	BioLegend
CD115-PE	FC	1:50	eBioscience	Rat IgG_{2A}	BioLegend

FC, flow cytometry; Neut, neutralization; biotin+, biotinylated.

recruitment at day 7 p.i. with numerous GFP^+ cells displaying microglial morphology. Microglial cell recruitment from the periphery was confirmed by the abundance of $CD45^{int}$ $CD11b^+GFP^+$ microglia isolated from day 7 p.i. cFMS-EGFP chimeras by flow cytometry. Furthermore, we found that most of these microglia expressed Gr1 at similar levels to those seen on circulating inflammatory monocytes, whereas a large majority of resident (GFP^-) microglia did not.

It has been shown that irradiation of the CNS may alter patterns of monocyte trafficking into the brain in synthetic models of CNS inflammation (10). Therefore, ability of $Ly6C^{hi}$ monocytes to traffic to the WNV-infected CNS in nonirradiated mice was confirmed using two different tracking techniques. First, we showed that adoptively transferred $Ly6C^{hi}$ BM-derived monocytes trafficked preferentially to the WNV-infected CNS, compared with $Ly6C^{lo}$ BM-derived monocytes. Although it may be argued that the use of BM-derived monocytes rather than blood-derived monocytes may skew the interpretation of our results, it is important to note that the outcome of the experiment further supports the role of inflammatory monocytes as microglial precursors. This is because $Ly6C^{hi}$ inflammatory monocytes also act as precursors for circulating monocytes, in which case they down-regulate Ly6C as they circulate (14, 49).

Furthermore, we stably labeled $Ly6C^{hi}$ inflammatory monocytes using a previously described method (14). We found during WNV encephalitis that FITC bead–labeled monocytes trafficked into the WNV-infected brain and developed a microglial phenotype, as determined by the expression of CD45, MHC-II, and CD86. Therefore, these data not only clearly show that inflammatory monocytes, rather than circulating monocytes, act as microglial precursors during WNV encephalitis but that inflammatory monocyte migration into the CNS does not require radiation preconditioning or obvious BBB disruption (10). Although our data conflict with previous reports showing that irradiation plays a critical role in the migration of monocyte-derived microglia, other studies suggest that irradiation does not cause any pathological changes in the brain (54, 55). Furthermore, the employment of head protection during irradiation not only protects the CNS from irradiation but also the large volume of blood within the brain, as well as the BM within the skull (56, 57). Although it remains to be seen what role these elements play in trafficking of monocytes into the brain, the findings outlined here in nonirradiated mice indicate that inflammatory monocyte trafficking is an event triggered by viral encephalitis, a scenario that has not previously been explored in this context.

Finally, similar increases in microglia are observed during WNV infection in mice devoid of the fractalkine receptor CX_3CR_1 (unpublished data), which further implicates inflammatory monocytes as microglial precursors. However, as CX_3CR_1 is expressed constitutively by resident microglia in the brain (58), further investigation into the relationship between microglia and $CX_3CR_1^+$-circulating monocytes is needed.

The trafficking of inflammatory monocytes has been linked to the expression of CCR2 and production of CCL2 (15, 16). WNV infection of the CNS resulted in significant amounts of CCL2 production. Neutralization of CCL2 resulted in a massive reduction of GFP^+ microglia in WNV-infected brains, clearly showing that the migration of inflammatory monocytes into the CNS is directed in part by the CCL2-CCR2 axis. However, the small number of GFP^+ cells that are still found to penetrate the WNV-infected brain after CCL2 neutralization suggests that the other CCR2 ligands, CCL7 and CCL12, may also play a role in this model (15, 16).

Investigation into the effects of CCL2 neutralization during WNV encephalitis on BM and circulating monocyte populations showed that CCL2 neutralization resulted in the retention of $Ly6C^{hi}$ monocytes both in the BM and circulating blood. This suggests, as shown previously in peripheral nonviral models, that CCL2 acts both at the level of BM

egress and also at the BBB interface (15, 16). It appears that the single-pulse antibody-mediated systemic reduction of the very high levels of CCL2, in the face of the high throughput of monocytes from the BM to the brain at this time point, may reduce immigration of monocytes into the brain before the effect of BM egress is apparent, causing an increase in blood monocyte numbers, which is in contrast to the effect of genetic absence of CCL2 (15).

The infiltration of $CD11b^+CD45^+$ myeloid cells has been implicated in the pathogenesis of WNV disease (21, 22). This has been argued to be because of infected infiltrating cells acting in a Trojan horse manner, enabling WNV entry from the periphery into the brain in association with breakdown of the BBB (21, 22, 59, 60). However, more recently it has been shown that WNV entry into the CNS is mediated via axonal transport (61), and integrity of the BBB does not necessarily predict disease outcomes (45). In our model of intranasal WNV infection, infectious virus can be isolated from the brain several days (day 3 p.i) before monocyte infiltration occurs (61, 62), which is consistent with the expression of CCL2 by infected neurons attracting monocytes into the brain from the bloodstream. Therefore, the observation that CCL2 neutralization prolongs the survival of infected mice, although apparently having no effect on viral titer, suggests that inflammatory monocyte-derived microglia are likely to play a pathogenic role in WNV encephalitis, which is not simply explained by their possible role in viral dissemination (61, 62).

It could be argued that the intranasal model of WNV infection is irrelevant in not mimicking natural infection. However, in all the published models of peripheral inoculation, the significant peripheral immune activation makes it impossible to separate the contribution of the systemic immune response to brain pathology that leads to death from the direct contribution of systemic immune response to death, independently of brain involvement. This is an important distinction that needs to inform interventional approaches to disease. The necessity of distinguishing experimentally between pathological events in the periphery and those in the brain has directed our development of this model. Furthermore, this distinction is likely to explain why macrophage deletion in peripheral inoculation results in enhanced mortality, whereas in our model it increases survival (63).

The exact role of microglia in immune-mediated pathology during WNV infection requires further investigation. Although it is likely that microglia secrete numerous proinflammatory cytokines, because we have shown the importance of glutamate excitotoxicity during WNV infection, we suggest that pathogenic functions of microglia may reside in differential roles of immigrant and resident microglia in regulating neuronal function. Although much work is required to prove this, when considering the exclusively neuronal localization of WNV (62) and the importance of microglia in regulating the neurological environment, it is not unreasonable to speculate that inflammatory monocyte-derived microglia may play a pathogenic role in this phenomenon. Our data cannot definitively rule out an important role for macrophages (that are also likely to be derived from inflammatory monocytes) or CCR2-expressing T cells in the pathogenesis of WNV encephalitis. However, work conducted by several independent groups suggests that macrophages and T cells, recruited in a CCR5-dependent manner, are important in viral clearance and do not drive immunopathology (19).

In conclusion, this is the first study to show that microglia are derived from inflammatory monocytes using CCL2 during a fatal model of flaviviral encephalitis. These exogenously derived microglia appear to bolster the endogenous microglial population. This CCL2-dependent migration appears to play a role in the pathogenesis of disease, as CCL2 neutralization prolonged the life of infected mice. The role of infiltrating inflammatory monocytes in mediating immunopathology during WNV encephalitis requires further investigation; however, their peripheral location before migration to the brain suggests that modulating these cells may serve as a novel therapy, not only during encephalitic disease but during other CNS disorders also.

MATERIALS AND METHODS

Virus propagation. As previously described (62), WNV (Sarafend) was derived from the brains of neonatal mice, which were used to infect confluent vero cell monolayers, at a multiplicity of infection of 5 PFU per cell. Infected cells were incubated for 40 h, after which they were frozen. Flasks were then thawed and the virus-rich supernatant clarified by centrifugation, after which aliquots were stored at −70°C until use.

Mice and infection. 8–16-wk-old female C57BL/6 (CD45.2) and congenic B6.SJL-$Ptprc^aPep3^b$/BoyJ (CD45.1), C57BL/6-7.2fms-EGFP transgenic (CD45.2) mice were obtained from the Blackburn animal house (University of Sydney, Sydney, Australia) or the Animal Resources Center (Western Australia). All procedures were performed with permission of the University of Sydney Animal Ethics Committee. All animals were housed under class II biohazard conditions in hepa filter-top cages. Food and water was provided ad libitum.

Intranasal infection was conducted as previously described with WNV 6×10^4 PFU in sterile PBS (Invitrogen). Sham infections were conducted by inoculating with sterile PBS only (62, 64).

Mice were killed using cardiac perfusion of anaesthetised mice with 40 ml of ice-cold PBS followed by perfusion with 20 ml of 4% PFA (Sigma-Aldrich) in PBS for histology or 50 ml PBS only for flow cytometry.

Plaque assay to determine viral titer. A virus plaque assay with virally susceptible BHK cells (donated by G. Karupiah, John Curtin Medical School, Canberra, Australia) was used. Tissue samples were dissected from animals and were immediately frozen in liquid nitrogen. 10% (wt/vol) tissues homogenates were prepared in Roswell Park Memorial Institute 1640 media (RPMI; CSL Biosciences) immediately before virus titration. In brief, thawed tissue samples were weighed in 2-ml screw cap tubes (SARSTEDT) before being disassociated with a power homogenizer (Tissue Tearor; BioSpec). The homogenates were then clarified by centrifugation at 1,500 rpm for 5 min at 4°C. The homogenate supernatant was used to infect BHK cells. Blood was collected from mice via the brachial artery. The samples were allowed to sit at 4°C for 8 h to coagulate before serum and plasma were separated by a high-speed 12,000 rpm centrifugation at 4°C. Supernatant serum was collected from centrifuged samples and stored in aliquots at −70°C.

BHK cells were seeded into 6-well plates at 1×10^6 cells per well in 2 ml RPMI overnight at 37°C in a 5% CO_2 incubator. Media was removed from the cells and replaced with 150 μl of virus samples at various dilutions.

For tissue samples, fivefold dilutions were prepared, whereas serum samples were titrated twofold only. One well per plate was reserved as a negative control. Plates were incubated and rocked every 15 min for 1 h at 37°C. The inoculum was removed by aspiration and the wells overlaid with 3 ml of 1.5% (wt/vol) low-gelling Agarose II (Amresco) in 2× MEM (Invitrogen). The agarose plugs were allowed to solidify before plates were incubated for a further 3 d at 37°C. After this period, wells were fixed with 3 ml of 10% formalin (Sigma-Aldrich) for 2 h before agarose plug removal. Fixation was necessary to kill free virus and to harden the agarose plug to facilitate removal. A 3% crystal violet (Hopkins and Williams) dye solution in 20% methanol (Fronine) was used to stain fixed cells. Excess crystal violet was washed off with PBS. Plates were dried overnight before plaques were counted using a colony counter (IUL, S. A.). The final PFU per gram (tissue) or milliliter (serum) was determined by factoring the number of plaques, the inoculum volume, and the dilution.

Generation of chimeric mice. 6–8-wk-old B6.SJL-PtprcaPep3b/BoyJ (CD45.1) mice were irradiated with one dose of 950 rads. 12 h later, mice were reconstituted with 10^7 donor BM cells from C57BL/6-7.2fms-EGFP BM. Mice were given sulfamethoxazole (Sigma-Aldrich) and trimethoprim (Sigma-Aldrich) in drinking water for 10 d after irradiation. 6–12 wk after irradiation, mice were infected with WNV as described in Mice and infection. Chimerism was checked using flow cytometry and was invariably found to be 96–99% of donor origin (Fig. S5).

Clodronate liposome depletion and FITC bead labeling of circulating monocytes. As previously shown, clodronate-encapsulated liposomes is an efficient method for depleting circulating macrophages (65–67). Clodronate was a gift of Roche. It was encapsulated in liposomes as described previously, and PBS-encapsulated liposomes were used as controls (65–67). Macrophages were depleted with multiple injections of clodronate-encapsulated liposomes on days 1, 3, and 5 after WNV infection. In the case of liposome tracking experiments, liposomes containing PBS were labeled with Dil (Invitrogen) and injected intravenously on day 7 p.i.

To label circulating monocytes, the previously described protocol (14, 50) was modified. C-L liposomes were injected i.v. on day 5.5 p.i. 12 h later, a second i.v. injection of FITC Flouresbrite polystyrene beads (Polyscience) diluted 1:25 in PBS was given. Control nonclodronate liposome treatment groups injected with PBS only or beads only were also used.

Immunohistology. As previously described (62), perfused brains and spleens were processed into paraffin blocks for sectioning. Sagittal 8-µm sections were cut for both routine H&E staining and IHC.

Antigen retrieval for WNV labeling was conducted as previously described (62). Antigen retrieval for lectin labeling was conducted using citrate buffer in a microwave oven set on 600 W for 8 min and allowed to cool for 25 min. Staining protocols for WNV antigen and lectin were identical and as previously described (62).

Fluorescence IHC was performed for the Gr1 complex with biotinylated Gr1 antibody (BioLegend) on cFMS-EGFP chimeras. In this case, brain tissue was fixed in 4% PFA at 4°C for 4 h and then immersed in 30% sucrose overnight, before being frozen in optimum cutting temperature compound (OCT; Tissue-Tek). 8-µm tissue sections were cut on a cryostat microtome and air dried. Fluorescence IHC was performed as previously described (62) with the addition of a tyramide-based amplification system (TSA kit; Perkin-Elmer) used according to the manufacturer's instructions.

The presence of D-L liposomes was investigated on frozen 8-µm brain and spleen sections. In addition, slides were incubated with FITC-conjugated lectin (Sigma-Aldrich) for 60 min before counter stain with DAPI antifade (Vector Laboratories).

BrdU incorporation. To detect proliferating cells, mice received 75 mg/kg BrdU (Becton Dickinson) i.v. 3 h before sacrifice on days 6 and 7 p.i. Proliferating cells were detected in situ by IHC using an anti-BrdU antibody on paraffin-embedded tissues (Skybio), as previously described (68). BrdU-positive cells were enumerated throughout the entire brain parenchyma on eight brains, two sections per brain, at days 6 and 7 p.i. from whole sagittal brain sections on double-blinded glass slides.

Microscope and image acquisition. Images were acquired on a microscope (BX-51; Olympus), using a camera (DP-70; Olympus) and DP manager 2.2.1 software (Olympus).

In-situ hybridization for CCL2. Paraffin-embedded sections were incubated with P^{33}-labeled cRNA probes transcribed from linearized plasmid constructs containing the CCL2 cDNA and processed for in situ hybridization histochemistry as described previously (61).

CNS leukocyte isolation. As previously described (69), leukocytes were obtained from the brains of infected mice by digesting brains in PBS with DNase (0.005 g/ml; Sigma-Aldrich) and collagenase IV (0.05 g/ml; Sigma-Aldrich) for 60 min at 37°C. Digestion was stopped with 10% FCS. The subsequent homogenate was passed through a nylon cell strainer with a 70-µm mesh size (Becton Dickinson). The pellet, obtained after 10-min centrifugation at 340 *g*, was resuspended in 30% percoll (GE Healthcare) and layered over 80% Percoll. Leukocytes were collected from the 30/80% interface after centrifugation at 1,140 *g* for 25 min at room temperature.

BM-derived monocyte and peripheral blood monocyte isolation. For flow cytometry analysis, the right femur was dissecting out and BM cells flushed out using PBS-loaded syringes. In the case of BM precursor isolation, femurs and tibias from at least four mice were used. The cellular suspension achieved after flushing was filtered through a 70-µm cell strainer and centrifuged for 5 min at 340 *g*. The red cells in the resulting pellet were lysed in NH_4Cl^- red cell lysis buffer before being centrifuged for 5 min at 340 *g*. In the case of peripheral blood, blood was collected via cardiac puncture immediately into citrate buffer (mmol; Sigma-Alrich). The resulting suspension was layered over 30% percoll and centrifuged at 1,140 *g* for 20 min at room temperature with the brake off. The interface was collected and the cells were washed once in PBS and centrifuged at 340 *g*.

Flow cytometry. Cells collected as described in the previous section from brain, blood, or BM were then washed in PBS and blocked with anti-CD16/CD32 (BioLegend) antibody. Viable cells were counted using trypan blue exclusion, which routinely showed >95% cell viability. The antibodies utilized for flow cytometry are outlined in Table I.

Cell surface molecule expression was measured and cell sorts were performed on a FACS ARIA (Becton Dickinson), equipped with an Argon ion and HeNe laser. Viable populations were gated by forward and side scatter and identified fluorescent populations determined by forward-gating thereafter. Sorting was performed using specific fluorescent and scatter parameters identifying the population of interest. Sorting stringencies was set to purity to achieve >98% purity for BM populations.

Acquired FACS data files were analyzed using the flow cytometry program Flow Jo (Tree Star, Inc.). Quantification of cell populations of interest were calculated based on flow cytometry percentages at analysis and absolute cell counts from each organ.

Adoptive transfer. We sorted both $Ly6C^{hi}$/cFMS-$EGFP^+$/$CD11b^+$ and $Ly6C^{lo}$/Cfms-$EGFP^+$/$CD11b^+$ populations from day 6 intranasally WNV-infected mice. $Ly6C^{hi}$ BM was labeled with 10 mM cell tracker orange (CMTMR [5-(and -6)-(((4-chloromethyl) benzoyl) amino) tetramethylrhodamine)-mixed isomers; Invitrogen). In brief, sorted cells were centrifuged and raised in 1 ml PBS containing 10 µM CMTMR. Cells were stained for 10 min before the reaction was stopped with 10% FCS. Cells were washed in 50 ml PBS at least three times. Labeled CMTMR $Ly6C^{hi}$ BM cells were then mixed 1:1 with $Ly6C^{lo}$ cells, which, except for the addition of CMTMR, had been treated similarly to $Ly6C^{hi}$ populations. A total of 2×10^6 BM cells were i.v. injected into either day 6.5 WNV-infected or mock-infected Ly5.1-C57BL/6 congenic mice. 12 h later, brains were

harvested as described in Mice and infection and CNS leukocyte isolation, and the presence of donor cells was investigated using flow cytometry, both using cFMS-EGFP and CMTMR–cell tracker orange.

CCL2 ELISA and neutralization. As previously described (62), cytokine bead arrays (Becton Dickinson) were used to measure CCL2 protein concentration in both serum and brain homogenates according to the manufacturer's instructions. CCL2 neutralization was conducted by giving 100 μg CCL2 (clone: 2H5; BioLegend) or isotype control (Hamster IgG; BioLegend) antibody injections i.p. late on days 5 and 6 consecutively. Late day 7 mice were killed and perfused, and PBMS, BMMC, and infiltrating CNS leukocytes were prepared as described as described in Mice and infection and CNS leukocyte isolation.

Statistics. Graphs were made and computerized statistical analysis was performed in Prism and InStat, respectively (both programs from GraphPad software, Inc.). Depending on the data, an unpaired, two-tailed Student's *t* test or one way ANOVA with a Tukey-Kramer post test was performed, with $P < 0.05$ considered to be significant.

Online supplemental material. Fig. S1 shows Lectin and NS-1 IHC on day 7 p.i. throughout the brain. Fig. S2 shows control labeling for BrdU by flow cytometry in microglia and T cells in the brain and $CD11b^+$ cells in BM in infected mice and in vitro–activated splenocytes. Fig. S3 shows Evans blue staining of the brain in WNV infection. Fig. S4 shows depletion of $Ly6C^{hi}$ and $Ly6C^{lo}$ monocytes in vivo by clodronate liposomes. Fig. S5 shows the purity of the cFMS-EGFP chimeras. Fig. S6 shows that acute CCL2 neutralization of mock-infected mice has no effect on monocyte populations. Online supplemental material is available at http://www.jem.org/cgi/content/full/jem.20080421/DC1.

We thank the members of the Blackburn animal house for their technical support and Barbara Hernandez for her time and help with histology in this paper.

This study was funded by the National Health and Medical Research Council (NHMRC 253771 and 512413) to N.J.C. King and National Institutes of Health grants (NS036979 and NS044905) to I.L. Campbell. D.R. Getts was in receipt of an Australian Postgraduate Award during this study. M. Muller was a postdoctoral fellow supported by the Deutsche Forschungsgemeinschaft (Mu17-07/3-1) and was also supported by the Innovative Medical Research fund of the University of Münster Medical School, Germany.

The authors do not have any conflicts of interest.

Submitted: 28 February 2008
Accepted: 8 August 2008

REFERENCES

1. Dalmau, I., J.M. Vela, B. Gonzalez, B. Finsen, and B. Castellano. 2003. Dynamics of microglia in the developing rat brain. *J. Comp. Neurol.* 458:144–157.
2. Fendrick, S.E., K.R. Miller, and W.J. Streit. 2005. Minocycline does not inhibit microglia proliferation or neuronal regeneration in the facial nucleus following crush injury. *Neurosci. Lett.* 385:220–223.
3. Lytle, J.M., and J.R. Wrathall. 2007. Glial cell loss, proliferation and replacement in the contused murine spinal cord. *Eur. J. Neurosci.* 25:1711–1724.
4. Pessac, B., I. Godin, and F. Alliot. 2001. Microglia: origin and development. *Bull. Acad. Natl. Med.* 185:337–346.
5. Djukic, M., A. Mildner, H. Schmidt, D. Czesnik, W. Bruck, J. Priller, R. Nau, and M. Prinz. 2006. Circulating monocytes engraft in the brain, differentiate into microglia and contribute to the pathology following meningitis in mice. *Brain.* 129:2394–2403.
6. Landsman, L., C. Varol, and S. Jung. 2007. Distinct differentiation potential of blood monocyte subsets in the lung. *J. Immunol.* 178:2000–2007.
7. Simard, A.R., and S. Rivest. 2004. Bone marrow stem cells have the ability to populate the entire central nervous system into fully differentiated parenchymal microglia. *FASEB J.* 18:998–1000.
8. Simard, A.R., D. Soulet, G. Gowing, J.P. Julien, and S. Rivest. 2006. Bone marrow-derived microglia play a critical role in restricting senile plaque formation in Alzheimer's disease. *Neuron.* 49:489–502.
9. Solomon, J.N., C.A. Lewis, B. Ajami, S.Y. Corbel, F.M. Rossi, and C. Krieger. 2006. Origin and distribution of bone marrow-derived cells in the central nervous system in a mouse model of amyotrophic lateral sclerosis. *Glia.* 53:744–753.
10. Mildner, A., H. Schmidt, M. Nitsche, D. Merkler, U.K. Hanisch, M. Mack, M. Heikenwalder, W. Bruck, J. Priller, and M. Prinz. 2007. Microglia in the adult brain arise from Ly-6C(hi)CCR2(+) monocytes only under defined host conditions. *Nat. Neurosci.* 10:1544–1553.
11. Rezaie, P., K. Patel, and D.K. Male. 1999. Microglia in the human fetal spinal cord–patterns of distribution, morphology and phenotype. *Brain Res. Dev. Brain Res.* 115:71–81.
12. Gehrmann, J., R.B. Banati, and G.W. Kreutzberg. 1993. Microglia in the immune surveillance of the brain: human microglia constitutively express HLA-DR molecules. *J. Neuroimmunol.* 48:189–198.
13. Geissmann, F., S. Jung, and D.R. Littman. 2003. Blood monocytes consist of two principal subsets with distinct migratory properties. *Immunity.* 19:71–82.
14. Tacke, F., F. Ginhoux, C. Jakubzick, N. van Rooijen, M. Merad, and G.J. Randolph. 2006. Immature monocytes acquire antigens from other cells in the bone marrow and present them to T cells after maturing in the periphery. *J. Exp. Med.* 203:583–597.
15. Serbina, N.V., and E.G. Pamer. 2006. Monocyte emigration from bone marrow during bacterial infection requires signals mediated by chemokine receptor CCR2. *Nat. Immunol.* 7:311–317.
16. Tsou, C.L., W. Peters, Y. Si, S. Slaymaker, A.M. Aslanian, S.P. Weisberg, M. Mack, and I.F. Charo. 2007. Critical roles for CCR2 and MCP-3 in monocyte mobilization from bone marrow and recruitment to inflammatory sites. *J. Clin. Invest.* 117:902–909.
17. Ginhoux, F., F. Tacke, V. Angeli, M. Bogunovic, M. Loubeau, X.M. Dai, E.R. Stanley, G.J. Randolph, and M. Merad. 2006. Langerhans cells arise from monocytes in vivo. *Nat. Immunol.* 7:265–273.
18. Diamond, M.S., B. Shrestha, A. Marri, D. Mahan, and M. Engle. 2003. B cells and antibody play critical roles in the immediate defense of disseminated infection by West Nile encephalitis virus. *J. Virol.* 77:2578–2586.
19. Glass, W.G., D.H. McDermott, J.K. Lim, S. Lekhong, S.F. Yu, W.A. Frank, J. Pape, R.C. Cheshier, and P.M. Murphy. 2006. CCR5 deficiency increases risk of symptomatic West Nile virus infection. *J. Exp. Med.* 203:35–40.
20. Wang, T., E. Scully, Z. Yin, J.H. Kim, S. Wang, J. Yan, M. Mamula, J.F. Anderson, J. Craft, and E. Fikrig. 2003. IFN-gamma-producing gamma delta T cells help control murine West Nile virus infection. *J. Immunol.* 171:2524–2531.
21. Arjona, A., H.G. Foellmer, T. Town, L. Leng, C. McDonald, T. Wang, S.J. Wong, R.R. Montgomery, E. Fikrig, and R. Bucala. 2007. Abrogation of macrophage migration inhibitory factor decreases West Nile virus lethality by limiting viral neuroinvasion. *J. Clin. Invest.* 117:3059–3066.
22. Wang, T., T. Town, L. Alexopoulou, J.F. Anderson, E. Fikrig, and R.A. Flavell. 2004. Toll-like receptor 3 mediates West Nile virus entry into the brain causing lethal encephalitis. *Nat. Med.* 10:1366–1373.
23. Sampson, B.A., C. Ambrosi, A. Charlot, K. Reiber, J.F. Veress, and V. Armbrustmacher. 2000. The pathology of human West Nile Virus infection. *Hum. Pathol.* 31:527–531.
24. Lawson, L.J., V.H. Perry, P. Dri, and S. Gordon. 1990. Heterogeneity in the distribution and morphology of microglia in the normal adult mouse brain. *Neuroscience.* 39:151–170.
25. Kreutzberg, G.W. 1995. Microglia, the first line of defence in brain pathologies. *Arzneimittelforschung.* 45:357–360.
26. Ponomarev, E.D., L.P. Shriver, K. Maresz, J. Pedras-Vasconcelos, D. Verthelyi, and B.N. Dittel. 2007. GM-CSF production by autoreactive T cells is required for the activation of microglial cells and the onset of experimental autoimmune encephalomyelitis. *J. Immunol.* 178:39–48.
27. Raivich, G., H. Bluethmann, and G.W. Kreutzberg. 1996. Signaling molecules and neuroglial activation in the injured central nervous system. *Keio J. Med.* 45:239–247.

28. Streit, W.J., M.B. Graeber, and G.W. Kreutzberg. 1988. Functional plasticity of microglia: a review. *Glia.* 1:301–307.
29. Trebst, C., S.M. Staugaitis, P. Kivisakk, D. Mahad, M.K. Cathcart, B. Tucky, T. Wei, M.R. Rani, R. Horuk, K.D. Aldape, et al. 2003. CC chemokine receptor 8 in the central nervous system is associated with phagocytic macrophages. *Am. J. Pathol.* 162:427–438.
30. Sedgwick, J.D., S. Schwender, H. Imrich, R. Dorries, G.W. Butcher, and V. ter Meulen. 1991. Isolation and direct characterization of resident microglial cells from the normal and inflamed central nervous system. *Proc. Natl. Acad. Sci. USA.* 88:7438–7442.
31. Banati, R.B., D. Hoppe, K. Gottmann, G.W. Kreutzberg, and H. Kettenmann. 1991. A subpopulation of bone marrow-derived macrophage-like cells shares a unique ion channel pattern with microglia. *J. Neurosci. Res.* 30:593–600.
32. Kraus, E., S. Schneider-Schaulies, M. Miyasaka, T. Tamatani, and J. Sedgwick. 1992. Augmentation of major histocompatibility complex class I and ICAM-1 expression on glial cells following measles virus infection: evidence for the role of type-1 interferon. *Eur. J. Immunol.* 22:175–182.
33. Vilhardt, F. 2005. Microglia: phagocyte and glia cell. *Int. J. Biochem. Cell Biol.* 37:17–21.
34. Carson, M.J., C.R. Reilly, J.G. Sutcliffe, and D. Lo. 1998. Mature microglia resemble immature antigen-presenting cells. *Glia.* 22:72–85.
35. Medana, I.M., T. Chan-Ling, and N.H. Hunt. 1996. Redistribution and degeneration of retinal astrocytes in experimental murine cerebral malaria: relationship to disruption of the blood-retinal barrier. *Glia.* 16:51–64.
36. Honda, M., H. Akiyama, Y. Yamada, H. Kondo, Y. Kawabe, M. Takeya, K. Takahashi, H. Suzuki, T. Doi, A. Sakamoto, et al. 1998. Immunohistochemical evidence for a macrophage scavenger receptor in Mato cells and reactive microglia of ischemia and Alzheimer's disease. *Biochem. Biophys. Res. Commun.* 245:734–740.
37. Henze, C., A. Hartmann, T. Lescot, E.C. Hirsch, and P.P. Michel. 2005. Proliferation of microglial cells induced by 1-methyl-4-phenylpyridinium in mesencephalic cultures results from an astrocyte-dependent mechanism: role of granulocyte macrophage colony-stimulating factor. *J. Neurochem.* 95:1069–1077.
38. Weissenbock, H., M. Hornig, W.F. Hickey, and W.I. Lipkin. 2000. Microglial activation and neuronal apoptosis in Bornavirus infected neonatal Lewis rats. *Brain Pathol.* 10:260–272.
39. Dallasta, L.M., L.A. Pisarov, J.E. Esplen, J.V. Werley, A.V. Moses, J.A. Nelson, and C.L. Achim. 1999. Blood-brain barrier tight junction disruption in human immunodeficiency virus-1 encephalitis. *Am. J. Pathol.* 155:1915–1927.
40. Eralinna, J.P., M. Soilu-Hanninen, M. Roytta, V. Hukkanen, A.A. Salmi, and R. Salonen. 1996. Blood-brain barrier breakdown and increased intercellular adhesion molecule (ICAM-1/CD54) expression after Semliki Forest (A7) virus infection facilitates the development of experimental allergic encephalomyelitis. *J. Neuroimmunol.* 66:103–114.
41. Gay, D., and M. Esiri. 1991. Blood-brain barrier damage in acute multiple sclerosis plaques. An immunocytological study. *Brain.* 114:557–572.
42. Luabeya, M.K., L.M. Dallasta, C.L. Achim, C.D. Pauza, and R.L. Hamilton. 2000. Blood-brain barrier disruption in simian immunodeficiency virus encephalitis. *Neuropathol. Appl. Neurobiol.* 26:454–462.
43. Mori, S., N.H. Sternberger, M.M. Herman, and L.A. Sternberger. 1991. Leakage and neuronal uptake of serum protein in aged and Alzheimer brains. A postmortem phenomenon with antemortem etiology. *Lab. Invest.* 64:345–351.
44. Soilu-Hanninen, M., J.P. Eralinna, V. Hukkanen, M. Roytta, A.A. Salmi, and R. Salonen. 1994. Semliki Forest virus infects mouse brain endothelial cells and causes blood-brain barrier damage. *J. Virol.* 68:6291–6298.
45. Morrey, J.D., A.L. Olsen, V. Siddharthan, N.E. Motter, H. Wang, B.S. Taro, D. Chen, D. Ruffner, and J.O. Hall. 2008. Increased blood-brain barrier permeability is not a primary determinant for lethality of West Nile virus infection in rodents. *J. Gen. Virol.* 89:467–473.
46. Tacke, F., and G.J. Randolph. 2006. Migratory fate and differentiation of blood monocyte subsets. *Immunobiology.* 211:609–618.
47. Bauer, J., I. Huitinga, W. Zhao, H. Lassmann, W.F. Hickey, and C.D. Dijkstra. 1995. The role of macrophages, perivascular cells, and microglial cells in the pathogenesis of experimental autoimmune encephalomyelitis. *Glia.* 15:437–446.
48. Polfliet, M.M., P.H. Goede, E.M. van Kesteren-Hendrikx, N. van Rooijen, C.D. Dijkstra, and T.K. van den Berg. 2001. A method for the selective depletion of perivascular and meningeal macrophages in the central nervous system. *J. Neuroimmunol.* 116:188–195.
49. Sunderkotter, C., T. Nikolic, M.J. Dillon, N. Van Rooijen, M. Stehling, D.A. Drevets, and P.J. Leenen. 2004. Subpopulations of mouse blood monocytes differ in maturation stage and inflammatory response. *J. Immunol.* 172:4410–4417.
50. Sasmono, R.T., D. Oceandy, J.W. Pollard, W. Tong, P. Pavli, B.J. Wainwright, M.C. Ostrowski, S.R. Himes, and D.A. Hume. 2003. A macrophage colony-stimulating factor receptor-green fluorescent protein transgene is expressed throughout the mononuclear phagocyte system of the mouse. *Blood.* 101:1155–1163.
51. Tacke, F., D. Alvarez, T.J. Kaplan, C. Jakubzick, R. Spanbroek, J. Llodra, A. Garin, J. Liu, M. Mack, N. van Rooijen, et al. 2007. Monocyte subsets differentially employ CCR2, CCR5, and CX3CR1 to accumulate within atherosclerotic plaques. *J. Clin. Invest.* 117:185–194.
52. Furtado, G.C., B. Pina, F. Tacke, S. Gaupp, N. van Rooijen, T.M. Moran, G.J. Randolph, R.M. Ransohoff, S.W. Chensue, C.S. Raine, and S.A. Lira. 2006. A novel model of demyelinating encephalomyelitis induced by monocytes and dendritic cells. *J. Immunol.* 177:6871–6879.
53. Hume, D.A. 2006. The mononuclear phagocyte system. *Curr. Opin. Immunol.* 18:49–53.
54. Yuan, H., M.W. Gaber, K. Boyd, C.M. Wilson, M.F. Kiani, and T.E. Merchant. 2006. Effects of fractionated radiation on the brain vasculature in a murine model: blood-brain barrier permeability, astrocyte proliferation, and ultrastructural changes. *Int. J. Radiat. Oncol. Biol. Phys.* 66:860–866.
55. Turrin, N.P., M.M. Plante, M. Lessard, and S. Rivest. 2007. Irradiation does not compromise or exacerbate the innate immune response in the brain of mice that were transplanted with bone marrow stem cells. *Stem Cells.* 25:3165–3172.
56. Mazo, I.B., J.C. Gutierrez-Ramos, P.S. Frenette, R.O. Hynes, D.D. Wagner, and U.H. von Andrian. 1998. Hematopoietic progenitor cell rolling in bone marrow microvessels: parallel contributions by endothelial selectins and vascular cell adhesion molecule 1. *J. Exp. Med.* 188:465–474.
57. Sipkins, D.A., X. Wei, J.W. Wu, J.M. Runnels, D. Cote, T.K. Means, A.D. Luster, D.T. Scadden, and C.P. Lin. 2005. In vivo imaging of specialized bone marrow endothelial microdomains for tumour engraftment. *Nature.* 435:969–973.
58. Cardona, A.E., E.P. Pioro, M.E. Sasse, V. Kostenko, S.M. Cardona, I.M. Dijkstra, D. Huang, G. Kidd, S. Dombrowski, R. Dutta, et al. 2006. Control of microglial neurotoxicity by the fractalkine receptor. *Nat. Neurosci.* 9:917–924.
59. Shen, J., S.S. T-To, L. Schrieber, and N.J. King. 1997. Early E-selectin, VCAM-1, ICAM-1, and late major histocompatibility complex antigen induction on human endothelial cells by flavivirus and comodulation of adhesion molecule expression by immune cytokines. *J. Virol.* 71:9323–9332.
60. King, N.J., D.R. Getts, M.T. Getts, S. Rana, B. Shrestha, and A.M. Kesson. 2007. Immunopathology of flavivirus infections. *Immunol. Cell Biol.* 85:33–42.
61. Samuel, M.A., H. Wang, V. Siddharthan, J.D. Morrey, and M.S. Diamond. 2007. Axonal transport mediates West Nile virus entry into the central nervous system and induces acute flaccid paralysis. *Proc. Natl. Acad. Sci. USA.* 104:17140–17145.
62. Getts, D.R., I. Matsumoto, M. Muller, M.T. Getts, J. Radford, B. Shrestha, I.L. Campbell, and N.J. King. 2007. Role of IFN-gamma in an experimental murine model of West Nile virus-induced seizures. *J. Neurochem.* 103:1019–1030.
63. Ben-Nathan, D., I. Huitinga, S. Lustig, N. van Rooijen, and D. Kobiler. 1996. West Nile virus neuroinvasion and encephalitis induced by macrophage depletion in mice. *Arch. Virol.* 141:459–469.
64. Wacher, C., M. Muller, M.J. Hofer, D.R. Getts, R. Zabaras, S.S. Ousman, F. Terenzi, G.C. Sen, N.J. King, and I.L. Campbell. 2007. Coordinated regulation and widespread cellular expression of interferon-stimulated genes (ISG) ISG-49, ISG-54, and ISG-56 in the central nervous system after infection with distinct viruses. *J. Virol.* 81:860–871.

65. van Rooijen, N., J. Bakker, and A. Sanders. 1997. Transient suppression of macrophage functions by liposome-encapsulated drugs. *Trends Biotechnol.* 15:178–185.
66. van Rooijen, N., and E. van Kesteren-Hendrikx. 2003. "In vivo" depletion of macrophages by liposome-mediated "suicide". *Methods Enzymol.* 373:3–16.
67. Van Rooijen, N., and A. Sanders. 1994. Liposome mediated depletion of macrophages: mechanism of action, preparation of liposomes and applications. *J. Immunol. Methods.* 174:83–93.
68. Muller, M., M. Stenner, K. Wacker, E.B. Ringelstein, W.F. Hickey, and R. Kiefer. 2006. Contribution of resident endoneurial macrophages to the local cellular response in experimental autoimmune neuritis. *J. Neuropathol. Exp. Neurol.* 65:499–507.
69. Muller, M., S.L. Carter, M.J. Hofer, P. Manders, D.R. Getts, M.T. Getts, A. Dreykluft, B. Lu, C. Gerard, N.J. King, and I.L. Campbell. 2007. CXCR3 signaling reduces the severity of experimental autoimmune encephalomyelitis by controlling the parenchymal distribution of effector and regulatory T cells in the central nervous system. *J. Immunol.* 179:2774–2786.